J|A|C|S ARTICLES

Published on Web 02/10/2010

Electronic Communication in Dinuclear C_4-Bridged Tungsten Complexes

Sergey N. Semenov, Olivier Blacque, Thomas Fox, Koushik Venkatesan, and Heinz Berke*

Department of Inorganic Chemistry, University of Zürich, Winterthurerstrasse 190, 8057 Zürich, Switzerland

Received November 17, 2009; E-mail: hberke@aci.uzh.ch

Abstract: The dinuclear tungsten carbyne $[X(CO)_2(dppe)WC_4W(dppe)(CO)_2X]$ (dppe = 1,2-bis(diphenylphosphino)ethane; X = I (**3**), Cl (**7**)) complexes were prepared from the bisacetylide precursor $Li_2[(CO)_3(dppe)WC_4W(CO)_3(dppe)]$ (**2**) via oxidative replacement of one CO group at each tungsten center with a halide substituent. The iodide ligand in **3** could be substituted with isothiocyanate or triflate resulting in $[X(CO)_2(dppe)WC_4W(dppe)(CO)_2X]$ complexes (X = NCS (**8**), OTf (**9**)). Substitution of two and all four CO ligands in **3** was achieved via subsequent photolytic or thermal activation with dppe. The "half-substituted" complex $[I(CO)_2(dppe)WC_4W(dppe)_2I]$ **(11)** allows reversible one-electron oxidation which results in the monocationic species $[I(CO)_2(dppe)WC_4W(dppe)_2I][PF_6]$ **(11[PF$_6$])**. The "all-dppe substituted" complex $[I(dppe)_2WC_4W(dppe)_2I]$ (**10**) possesses two reversible redox states leading to the stable monocationic $[I(dppe)_2WC_4W(dppe)_2I][PF_6]$ (**10[PF$_6$]**) and the dicationic $[I(dppe)_2WC_4W(dppe)_2I][PF_6]_2$ (**10[PF$_6$]$_2$**) compounds. The complexes **2**, **3**, $[W(CO)_3(dppe)(C{\equiv}CPh)(I)]$ (**4**), $[X(CO)_2(dppe)W{\equiv}C-C(Me){=}C(Me)-C{\equiv}W(dppe)(CO)_2X]$ (X = I (**5**), Cl (**6**)), **7**, **8**, **10**, **11** and **11[PF$_6$]** were characterized by single crystal X-ray diffraction. The electronic properties of complexes **10**, **10[PF$_6$]**, **10[PF$_6$]$_2$**, as well as of compounds **11** and **11[PF$_6$]**, were investigated using cyclic voltammetry (CV), EPR, IR, near-IR spectroscopy, and magnetization measurements. These studies showed that the [W]≡C−C≡C−C≡[W] canonical form of the bridged system with strong tungsten−carbon interaction contributes significantly to the electronic coupling in the mixed-valent species **10[PF$_6$]** (comproportionation constant $K_c = 7.5 \times 10^4$) and to the strong antiferromagnetic coupling in the dicationic complex **10[PF$_6$]$_2$** (exchange integral $J = -167$ cm^{-1}). In addition, the rate for electron transfer between the tungsten centers in **10[PF$_6$]** was evaluated by near-IR and IR studies.

Introduction

Organometallic dinuclear metal complexes of the type $[L_nMC_xML_n]$ (M = metal; L = ligand) are thought to have great potential for their application as devices in molecular electronics. Among other aspects these abilities are based on their basic function of "single-electron" conductance across the linear, unsaturated carbon bridge and on their redox-active end groups lending electrons for through-bridge travel. Such type of compounds in particular can potentially function as a molecular wire. Molecular wires constitute the basis for the construction of field-effect transistors and diodes. In addition to this their mixed valent states are exceptional models for electron transfer studies.[1−5] The complexes with $n = 4$ are the most ubiquitous of these series of complexes and have been reported for Mn,[6] Fe,[7,8] Re,[9] Ru,[10,11] Pt,[12] W and Mo centers.[13,14] The electronics and structures of the C_4 chain correspond for most complexes to the acetylenic butadiynediyl canonical form, but for rarer other cases they correspond to the cumulenic butatrienebisylidene form (Scheme 1).

There are only two examples of a carbyne-type butynebis(triyl) bridge reported for related W and Mo complexes.[13] The C_4 chain has been demonstrated as one of the most efficient bridges for electronic communication between metal centers due to the presence of two transmitting π-systems and their propensity for polarization.[8] These complexes therefore often show high degrees of electron delocalization resulting in efficient stabilization of mixed-valence species. Various such complexes possess low thermal and air stability, which would limit their application in molecular electronics and hinder also attempts for further buildup of oligonuclears based on such systems. The most common and well-documented end groups are the

Scheme 1. Canonical Forms of a C_4 Unit in $[M]C_4[M]$ Structures

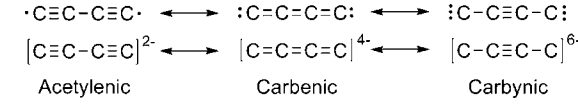

(1) (a) Carroll, L. R.; Gorman, B. C. *Angew. Chem., Int. Ed.* **2002**, *41*, 4378–4400. (b) Joachim, C.; Gimzewski, J. K.; Aviram, A. *Nature* **2000**, *408*, 541–548. (c) Chen, F.; Hihath, J.; Huang, Z. F.; Li, X. L.; Tao, N. J. *Annu. Rev. Phys. Chem.* **2007**, *58*, 535–564. (d) Tao, N. J. *Nature Nanotechnol.* **2006**, *1*, 173–181. (e) Nitzan, A.; Ratner, M. A. *Science* **2003**, *300*, 1384–1389. (f) Zhirnov, V. V.; Cavin, R. K. *Nat. Mater.* **2006**, *5*, 11–12. (g) Park, J.; Pasupathy, A. N.; Goldsmith, J. I.; Chang, C.; Yaish, Y.; Petta, J. R.; Rinkoski, M.; Sethna, J. P.; Abruna, H. D.; McEuen, P. L.; Ralph, D. C. *Nature* **2002**, *417*, 722–725. (h) Liang, W. J.; Shores, M. P.; Bockrath, M.; Long, J. R.; Park, H. *Nature* **2002**, *417*, 725–729. (i) Tuccitto, N.; Ferri, V.; Cavazzini, M.; Quici, S.; Zhavnerko, G.; Licciardello, A.; Rampi, M. A. *Nat. Mater.* **2009**, *8*, 41–46. (j) Low, P. J. *Dalton Trans.* **2005**, 2821–2824. (k) Paul, F.; Lapinte, C. *Coord. Chem. Rev.* **1998**, 178–180, 431−509.

[Re(NO)(Cp)(PPh_3)] and [Fe(dppe)(Cp*)] moieties.[15] These units, however, represent stopper functions that provide no functionality for a hook-up to electrodes or for further extension of these systems to form oligonuclears. The acetylenic or cumulenic chemistry of platinum has been extensively reported;[16,17] however, Pt compounds do not normally provide suitable redox properties for single-electron conductance. Moreover, in π-delocalized Pt(II) systems, delocalization is often interrupted at the metal center, which may hinder the electron travel in single-molecule junctions.[18] Ruthenium complexes with fragments [$Ru(P_2)_2$], P_2 = dppe and dppm (dppm = 1,2-bis(diphenylphosphino)methane) seem to offer the right balance between electronic delocalization and redox properties, and stability required for applications.[19] Such complexes were therefore used in single-layer capacity studies and recently also in single-electron conductance measurements.[20] However, the absence of new metal end groups with an appropriate combination of properties seems to currently impede further progress in the field.

Bridged complexes with emphasis on the carbyne canonical forms [$L_nM]C_4[ML_n$] are expected to possess higher stability and the possibility for facile synthetic modifications.[21−25] Carbyne-type canonical forms promise strong involvement of metal orbitals in the π-conjugated systems with the possibility for a tuning of spectroscopic, in particular NLO (nonlinear optical), properties.[25−29] Organometallic polymers based on such type of building blocks connected by bisacetylides have great implications, since these compounds retain conjugation along the backbone.[25,27] Mononuclear tungsten Fischer-type carbyne complexes are relatively common species, and several preparative methods were developed for their synthesis.[22,23,27,30−32] However, dinuclear C_4-bridged complexes with emphasis on the carbyne structure are rare except for [W]C_4[W] and [Mo]C_4[Mo] systems.[13] These compounds were synthesized using relatively complex procedures starting from mononuclear precursors utilizing the oxidative coupling of C_2 units to build the C_4 bridges. Physical characterization of these complexes have been limited to CV studies.[33] Moreover, these complexes have stopper-type termini not prone to further chemical func-

(2) Brunschwig, B. S.; Sutin, N. *Coord. Chem. Rev.* **1999**, *187*, 233–254.
(3) Demadis, D. D.; Hartshorn, C. M.; Meyer, T. J. *Chem. Rev.* **2001**, *101*, 2655–2685.
(4) Ward, M. D.; McCleverty, J. A. *Dalton Trans.* **2002**, 275.
(5) Kaim, W.; Klein, A.; Glockle, M. *Acc. Chem. Res.* **2000**, *33*, 755–763.
(6) (a) Kheradmandan, S.; Heinze, K.; Schmalle, H. W.; Berke, H. *Angew. Chem., Int. Ed.* **1999**, *38*, 2270–2273. (b) Venkatesan, K.; Fox, T.; Schmalle, H. W.; Berke, H. *Organometallics* **2005**, *24*, 2834–2847. (c) Venkatesan, K.; Fernandez, F. J.; Blacque, O.; Fox, T.; Alfonso, M.; Schmalle, H. W.; Berke, H. *Chem. Commun.* **2003**, 2006–2008.
(7) Lenarvor, N.; Toupet, L.; Lapinte, C. *J. Am. Chem. Soc.* **1995**, *117*, 7129–7138.
(8) Jiao, H. J.; Costuas, K.; Gladysz, J. A.; Halet, J. F.; Guillemot, M.; Toupet, L.; Paul, F.; Lapinte, C. *J. Am. Chem. Soc.* **2003**, *125*, 9511–9522.
(9) (a) Brady, M.; Weng, W. Q.; Zhou, Y. L.; Seyler, J. W.; Amoroso, A. J.; Arif, A. M.; Bohme, M.; Frenking, G.; Gladysz, J. A. *J. Am. Chem. Soc.* **1997**, *119*, 775–788. (b) Zhou, Y. L.; Seyler, J. W.; Weng, W. Q.; Arif, A. M.; Gladysz, J. A. *J. Am. Chem. Soc.* **1993**, *115*, 8509–8510. (c) Yam, V. W. W.; Lau, V. C. Y.; Cheung, K. K. *Organometallics* **1996**, *15*, 1740–1744.
(10) Paul, F.; Meyer, W. E.; Toupet, L.; Jiao, H. J.; Gladysz, J. A.; Lapinte, C. *J. Am. Chem. Soc.* **2000**, *122*, 9405–9414.
(11) Bruce, M. I.; Low, P. J.; Costuas, K.; Halet, J. F.; Best, S. P.; Heath, G. A. *J. Am. Chem. Soc.* **2000**, *122*, 1949–1962.
(12) Onitsuka, K.; Ose, N.; Ozawa, F.; Takahashi, S. *J. Organomet. Chem.* **1999**, *578*, 169–177.
(13) Woodworth, B. E.; White, P. S.; Templeton, J. L. *J. Am. Chem. Soc.* **1997**, *119*, 828–829.
(14) Roberts, R. L.; Puschmann, H.; Howard, J. A. K.; Yamamoto, J. H.; Carty, A. J.; Low, P. J. *Dalton Trans.* **2003**, 1099–1105.
(15) (a) Ibn Ghazala, S.; Paul, F.; Toupet, L.; Roisnel, T.; Hapiot, P.; Lapinte, C. *J. Am. Chem. Soc.* **2006**, *128*, 2463–2476. (b) Coat, F.; Lapinte, C. *Organometallics* **1996**, *15*, 477–479. (c) Bartik, T.; Bartik, B.; Brady, M.; Dembinski, R.; Gladysz, J. A. *Angew. Chem., Int. Ed. Engl.* **1996**, *35*, 414–417. (d) Dembinski, R.; Bartik, T.; Bartik, B.; Jaeger, M.; Gladysz, J. A. *J. Am. Chem. Soc.* **2000**, *122*, 810–822.
(16) (a) Zheng, Q. L.; Gladysz, J. A. *J. Am. Chem. Soc.* **2005**, *127*, 10508–10509. (b) Farley, R. T.; Zheng, Q. L.; Gladysz, J. A.; Schanze, K. S. *Inorg. Chem.* **2008**, *47*, 2955–2963.
(17) Zhuravlev, F.; Gladysz, J. A. *Chem.—Eur. J.* **2004**, *10*, 6510–6522.
(18) (a) Mayor, M.; von Hanisch, C.; Weber, H. B.; Reichert, J.; Beckmann, D. *Angew. Chem., Int. Ed.* **2002**, *41*, 1183–1186. (b) Schull, T. L.; Kushmerick, J. G.; Patterson, C. H.; George, C.; Moore, M. H.; Pollack, S. K.; Shashidhar, R. *J. Am. Chem. Soc.* **2003**, *125*, 3202–3203.
(19) (a) Rigaut, S.; Perruchon, J.; Le Pichon, L.; Touchard, D.; Dixneuf, P. H. *J. Organomet. Chem.* **2003**, *670*, 37–44. (b) Touchard, D.; Haquette, P.; Guesmi, S.; LePichon, L.; Daridor, A.; Toupet, L.; Dixneuf, P. H. *Organometallics* **1997**, *16*, 3640–3648. (c) Rigaut, S.; Massue, J.; Touchard, D.; Fillaut, J. L.; Golhen, S.; Dixneuf, P. H. *Angew. Chem., Int. Ed.* **2002**, *41*, 4513–4517. (d) Rigaut, S.; Le Pichon, L.; Daran, J. C.; Touchard, D.; Dixneuf, P. H. *Chem. Commun.* **2001**, 1206–1207. (e) Rigaut, S.; Olivier, C.; Costuas, K.; Choua, S.; Fadhel, O.; Massue, J.; Turek, P.; Saillard, J. Y.; Dixneuf, P. H.; Touchard, D. *J. Am. Chem. Soc.* **2006**, *128*, 5859–5876.
(20) (a) Qi, H.; Gupta, A.; Noll, B. C.; Snider, G. L.; Lu, Y. H.; Lent, C.; Fehlner, T. P. *J. Am. Chem. Soc.* **2005**, *127*, 15218–15227. (b) Liu, K.; Wang, X. H.; Wang, F. S. *ACS Nano* **2008**, *2*, 2315–2323.
(21) (a) Frank, K. G.; Selegue, J. P. *J. Am. Chem. Soc.* **1990**, *112*, 6414–6416. (b) Dewhurst, R. D.; Hill, A. F.; Willis, A. C. *Organometallics* **2009**, *28*, 4735–4740. (c) Schrock, R. R. *Chem. Rev.* **2002**, *102*, 145–179. (d) Herndon, J. W. *Coord. Chem. Rev.* **2009**, *253*, 86–179. (e) Jeffery, J. C.; Weller, A. S. *J. Organomet. Chem.* **1997**, *548*, 195–203. (f) Dewhurst, R. D.; Hill, A. F.; Rae, A. D.; Willis, A. C. *Organometallics* **2005**, *24*, 4703–4706. (g) Dewhurst, R. D.; Hill, A. F.; Smith, M. K. *Organometallics* **2005**, *24*, 5576–5580. (h) Atagi, L. M.; Critchlow, S. C.; Mayer, J. M. *J. Am. Chem. Soc.* **1992**, *114*, 9223–9224. (i) Bannwart, E.; Jacobsen, H.; Furno, F.; Berke, H. *Organometallics* **2000**, *19*, 3605–3619. (j) Furno, F.; Fox, T.; Schmalle, H. W.; Berke, H. *Organometallics* **2000**, *19*, 3620–3630. (k) Mayr, A.; Dorries, A. M.; Mcdermott, G. A.; Vanengen, D. *Organometallics* **1986**, *5*, 1504–1506.
(22) (a) Mcdermott, G. A.; Dorries, A. M.; Mayr, A. *Organometallics* **1987**, *6*, 925–931. (b) Zhang, L.; Gamasa, M. P.; Gimeno, J.; Carbajo, R. J.; López-Ortiz, F.; Lanfranchi, M.; Tiripicchio, A. *Organometallics* **1996**, *15*, 4274–4284.
(23) Yu, M. P. Y.; Cheung, K. K.; Mayr, A. *J. Chem. Soc., Dalton Trans.* **1998**, 2373–2378.
(24) Yu, M. P. Y.; Yam, V. W. W.; Cheung, K. K.; Mayr, A. *J. Organomet. Chem.* **2006**, *691*, 4514–4531.
(25) Manna, J.; Geib, S. J.; Hopkins, M. D. *J. Am. Chem. Soc.* **1992**, *114*, 9199–9200.
(26) Powell, C. E.; Humphrey, M. G. *Coord. Chem. Rev.* **2004**, *248*, 725–756.
(27) John, K. D.; Hopkins, M. D. *Chem. Commun.* **1999**, 589–590.
(28) (a) Mayr, A.; Yu, M. P. Y.; Yam, V. W. W. *J. Am. Chem. Soc.* **1999**, *121*, 1760–1761. (b) Da Re, R. E.; Hopkins, M. D. *Coord. Chem. Rev.* **2005**, *249*, 1396–1409.
(29) Xu, Z. H.; Mayr, A.; Butler, I. S. *J. Organomet. Chem.* **2002**, *648*, 93–98.
(30) (a) Pollagi, T. P.; Geib, S. J.; Hopkins, M. D. *J. Am. Chem. Soc.* **1994**, *116*, 6051–6052. (b) Mayr, A.; Asaro, M. F.; Kjeisberg, M. A.; Lee, K. S.; Van Engen, D. *Organometallics* **1987**, *6*, 432–434. (c) Mayr, A.; Mcdermott, G. A. *J. Am. Chem. Soc.* **1986**, *108*, 548–549. (d) Birdwhistell, K. R.; Burgmayer, S. J. N.; Templeton, J. L. *J. Am. Chem. Soc.* **1983**, *105*, 7789–7790. (e) Sharp, P. R.; Holmes, S. J.; Schrock, R. R.; Churchill, M. R.; Wasserman, H. J. *J. Am. Chem. Soc.* **1981**, *103*, 965–966. (f) Atagi, L. M.; Critchlow, S. C.; Mayer, J. M. *J. Am. Chem. Soc.* **1992**, *114*, 1483–1484.
(31) Schwenzer, B.; Schleu, J.; Burzlaff, N.; Karl, C.; Fischer, H. *J. Organomet. Chem.* **2002**, *641*, 134–141.
(32) Birdwhistell, K. R.; Tonker, T. L.; Templeton, J. L. *J. Am. Chem. Soc.* **1985**, *107*, 4474–4483.
(33) Frohnapfel, D. S.; Woodworth, B. E.; Thorp, H. H.; Templeton, J. L. *J. Phys. Chem. A* **1998**, *102*, 5665–5669.

Scheme 2

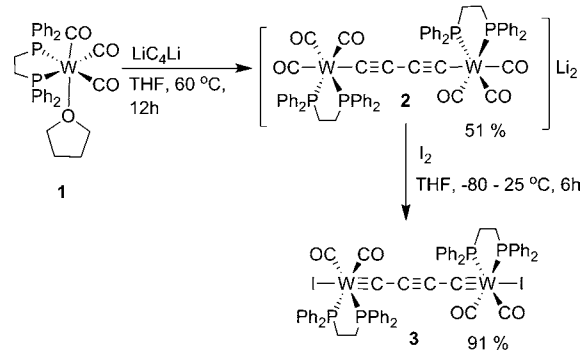

Scheme 3

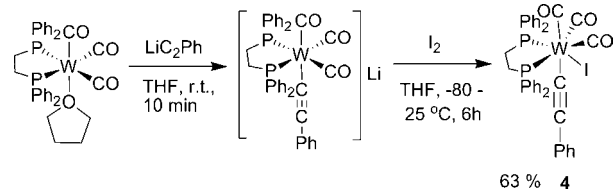

Scheme 4

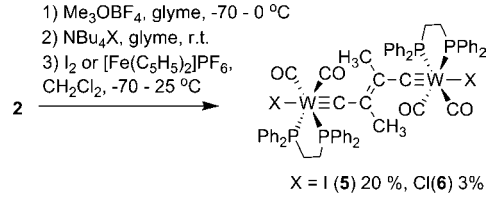

Scheme 5

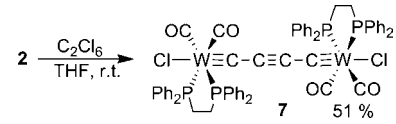

tionalization. In this paper we demonstrate facile synthetic access to tungsten complexes with delocalized, preferably carbyne-type $[W]C_4[W]$ structures where [W] is $[(X)W(dppe)(CO)_2]$, $[(X)W(dppe)_2]$, and replaceable X groups. A thorough study is sought to unravel the physical properties of these complexes for proper pre-evaluation prior to measurements of single-electron conductance.

Results and Discussion

Synthesis and Characterization of Complexes. Substitution reactions of *fac*-$W(CO)_3$(dppe)(L) (L = acetone, THF) complexes with lithium acetylides were explored earlier as routes to access the corresponding tungsten acetylide species.[32,34] In these studies the *fac*-$W(CO)_3$(dppe)(acetone) intermediate could not be used, since it was necessary to avoid acetone in the reaction mixture; instead the *fac*-$W(CO)_3$(dppe)(THF) complex (**1**) turned out to be more feasible because the released THF does not have any impact on the reaction. It was isolated in 55% yield after two steps starting from $W(CO)_6$ and could be stored at −30 °C over long periods of time.[35] As depicted in Scheme 2, subsequent reaction of **1** with solid $[Li_2C_4(THF)_n]$[36] gave the key compound $Li_2[(CO)_3(dppe)W(C{\equiv}CC{\equiv}C)W(dppe)(CO)_3]$ (**2**) in 51% yield upon precipitation with benzene. Attempts to use *in situ* generated lithium salt, Li_2C_4, obtained from $Me_3SiC{\equiv}CC{\equiv}CSiMe_3$ and MeLi·LiBr produced side reactions and thus gave lower yields in comparison with the utilization of solid $[Li_2C_4(THF)_n]$. The ^{13}C NMR spectrum of **2** showed two resonances for the C_4 chain at 106.2 (C_α) and 106.9 (C_β) ppm. In the IR spectra typical $\nu(C{\equiv}O)$ bands were observed at 1892, 1814, and 1727 cm^{-1}. The band positions were similar to those of the previously reported $M[W(dppe)(CO)_3(C{\equiv}CR)]$ (M = Li, Na; R = Ph, Me, H) series.[32]

Conversion of **2** into the $[I(CO)_2(dppe)WC_4W(dppe)(CO)_2I]$ complex **3** as indicated in Scheme 2 was effected by oxidation with 2 equiv of I_2. The reaction from **2** to **3** was anticipated to involve single-electron oxidation steps, loss of CO, and coordination of iodide or I^+ transfer at each tungsten center. **3** was obtained as air-stable violet crystals in 80% yield and was fully characterized by NMR, IR spectroscopy, and elemental analysis. A carbyne-type structure was presumed. The C_α and C_β resonances appear as triplets at 225.2 and 87.5 ppm with $^2J(^{13}C,^{31}P)$ = 11.1 Hz and $^3J(^{13}C,^{31}P)$ = 3.7 Hz, respectively. The C_α resonances were shifted high field in comparison with many of the reported mononuclear tungsten carbyne complexes, indicating changes in the electronic structure.[24,25,32] The ^{31}P NMR spectrum showed a superimposed singlet (W nucleus not magnetically active) and doublet at 29.3 ppm with $^1J(^{31}P,^{183}W)$ = 228 Hz. The oxidative transformation to **3** is unprecedented. A related type of transformation was put forward for $[RuC_4Ru]^{0-4+}$ systems, but was never clearly confirmed.[11] In order to trace the intermediates of the conversion of **2** to **3**, a "model" reaction between $Li[W(CO)_3(dppe)(C{\equiv}CPh)]$ and one equivalent of I_2 was carried out, which was found to proceed via a seven-coordinated $[W(CO)_3(dppe)(C{\equiv}CPh)(I)]$ complex (**4**) (Scheme 3). On the basis of these observations the formation of $[(CO)_3(dppe)(I)WC_4W(I)(dppe)(CO)_3]$ is invoked as a primary intermediate in the formation of **3**.

According to Scheme 4, compound **2** was reacted with electrophiles. Treatment of **2** with Me_3OBF_4 in the presence of NBu_4X (X = Cl, I) with subsequent oxidation by I_2 or $[FeCp_2][PF_6]$ gave the neutral complexes **5** and **6**. This reaction is thought to involve the intermediate $[X(CO)_2(dppe)W{\equiv}C{-}C(Me){=}C(Me){-}C{\equiv}W(dppe)(CO)_2X][NBu_4]_2$ presumably resulting from a sequence of electrophilic attacks by Me_3O^+ followed by rearrangement of the bridge to the carbyne form and subsequent substitution of CO activated by the *trans* effect of carbyne as was found in mononuclear complexes.[32,37]

A chloride derivative $[Cl(CO)_2(dppe)WC_4W(dppe)(CO)_2Cl]$ (**7**) analogous to **3** was obtained in 15% yield upon treatment of **2** with chloroform or in 51% yield applying chlorination with C_2Cl_6 (Scheme 5).

We then sought to utilize **3** and **7** for variation of the axial groups by substitution with labile anionic ligands. The best results were achieved using silver salts due to concomitant enforcement of the halogen abstraction (Scheme 6). Since N-bound isothiocyanate ligands could principally be used for the anchoring of such molecules via sulfur coordination to gold surfaces as required for measurements of single-electron-

(34) Roth, G.; Fischer, H. *Organometallics* **1996**, *15*, 1139–1145.
(35) Birdwhistell, K. R.; Dema, A. C.; Li, X.; Lukehart, C. M.; Owen, M. D. *Inorg. Synth.* **1992**, *29*, 141–146.
(36) Werz, D. B.; Gleiter, R.; Rominger, F. *J. Am. Chem. Soc.* **2002**, *124*, 10638–10639.
(37) Mayr, A.; Schaefer, K. C.; Huang, E. Y. *J. Am. Chem. Soc.* **1984**, *106*, 1517–1518.

Scheme 6

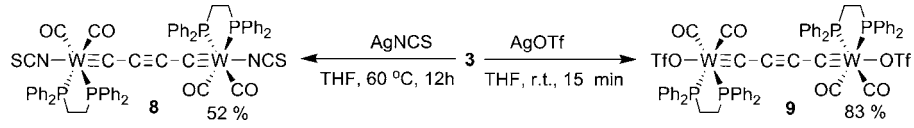

Scheme 7

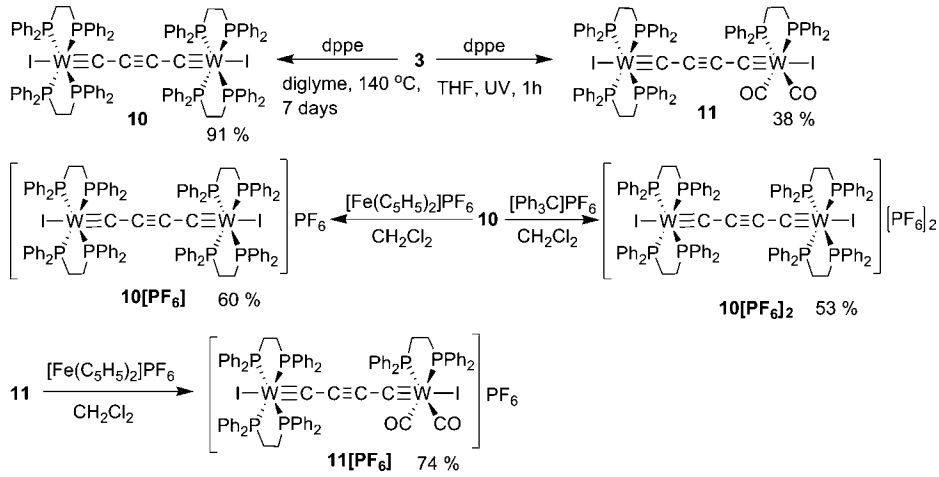

conductivities,[38] the heterogeneous reaction of a THF solution of **3** with AgSCN was carried out, which indeed afforded the isothiocyanate derivative [SCN(CO)$_2$(dppe)WC$_4$W(dppe)-(CO)$_2$NCS] (**8**). The N-coordination was assigned on the basis of υ (NCS) observed at 2034 cm^{-1}. Bands lower than 2100 cm^{-1} are more typical for isothiocyanates (N-coordination) derivatives,[39] and the structure was further confirmed by X-ray analysis. The reaction with silver triflate gave the corresponding substituted product [(OTf)(CO)$_2$(dppe)WC$_4$W-(dppe)(CO)$_2$(OTf)] (**9**) in 83% yield.

The spectroscopic properties of **7**−**9** overall resemble those of **3**. For instance the ^{31}P NMR shifts are similar to those of mononuclear tungsten carbynes, and the $^1J_{W-P}$ coupling constants were only slightly affected by the new substituent in the axial positions.[25,27,32] The C$_\beta$ resonances of the symmetrical molecules **3** and **7**−**9** shift monotonically downfield with a decreasing size of the ligand *trans* to the C$_4$ chain. This behavior is consistent with an increase of the WC$_\alpha$ bond lengths from **3** to **8** and might be related to an increase in the π-acceptor property on going from I$^-$ to NCS$^-$. A similar behavior was observed in the [XW(PMe$_3$)$_4$(CH)] series.[40] The C$_\beta$ resonances of **3** and **7**−**9** shift monotonically highfield from I$^-$ to OTf$^-$.

The IR spectra exhibit two characteristic absorptions for the C≡O vibrations in the range of 2000−1925 cm^{-1}. These ν(C≡O) are shifted to lower energies with respect to the comparable mononuclear compounds [(X)(CO)$_2$(dppe)WC−R],[23,29,31] which might be due to a increase in electron density on the metal center and a concomitant weaker tungsten-to-carbon bond in **3** and **7**−**9**. The ν(C≡O) bands of **3** show a slight high energy shift upon substitution of the iodine ligands by chlorides and by about 15 cm^{-1} upon substitution with the OTf.

CV studies on the complexes **3** and **7**−**9** revealed irreversible oxidation behavior, which was thought to be due to the presence of the CO ligands becoming labile in higher oxidation states of the tungsten centers. Indeed, CO-containing carbyne compounds of the type [W(CR)(CO)$_n$L$_{4-2n}$X] typically showed electrochemically irreversible behavior.[24] However, mononuclear "all-phosphine"-substituted complexes of the type [W(CR)(PP)$_2$X] possess reversible redox processes.[41]

In order to fine-tune the electrochemical properties of such types of compounds to the requirements of the redox wires, the substitution of the CO ligands of **3** with dppe was attempted by thermal and photolytic activation (Scheme 7). UV irradiation of **3** produced the unsymmetrically substituted complex [I(CO)$_2$(dppe)WC$_4$W(dppe)$_2$I] (**11**), which showed four different ^{13}C NMR signals for the carbon chain at 230.3, 212.3, 93.9, and 83.0 ppm. However, approaching exhaustive CO substitution of **3** by extended UV irradiation led to degradation of **11**. Substitution of all four CO molecules could eventually be effected by heating compound **3** to 140 °C in diglyme with intermittent removal of the evolved CO applying vacuum. The desired product [I(dppe)$_2$WC$_4$W(dppe)$_2$I] (**10**) precipitated during the course of the reaction as large dark-green crystals in 85−90% yield. In contrast to the previously discussed complexes, **10** furnished a broad ^{31}P NMR signal at around 45 ppm. The ^{13}C NMR spectrum revealed sharp signals for the C$_\alpha$ and C$_\beta$ nuclei, but broad lines for *ipso*-C$_6$H$_5$ carbon atoms. The broadening was attributed to ligand dynamics confirmed by variable-temperature ^{31}P NMR studies as shown in Figure 1. The initially broad ^{31}P NMR signal splits upon lowering the temperature into four doublets, two of which overlap. Phosphorus nuclei in *trans* positions are known to couple more strongly than the nuclei in *cis* positions. Hence, the coupling constants of $^2J_{P-P} \approx 120$ Hz can be attributed to the phosphorus nuclei in the *trans* position. We assume an arrangement of four inequivalent "in-plane" phosphorus nuclei due to the tilting distortion of the square pyramid formed by the four phosphorus nuclei and the C$_\alpha$. This could be attributed from the crystal structure, where the P$_4$ plane is not fully perpendicular to the

(38) Han, W. H.; Durantini, E. N.; Moore, T. A.; Moore, A. L.; Gust, D.; Rez, P.; Leatherman, G.; Seely, G. R.; Tao, N. J.; Lindsay, S. M. *J. Phys. Chem. B* **1997**, *101*, 10719–10725.
(39) Sabatini, A.; Bertini, I. *Inorg. Chem.* **1965**, *4*, 1665–1667.
(40) Holmes, S. J.; Schrock, R. R.; Churchill, M. R.; Wasserman, H. J. *Organometallics* **1984**, *3*, 476–484.
(41) van der Eide, E. F.; Piers, W. E.; Parvez, M.; McDonald, R. *Inorg. Chem.* **2007**, *46*, 14–21.

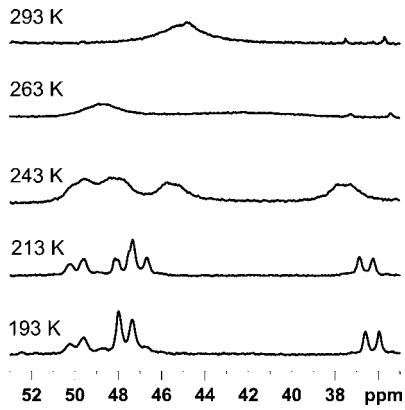

Figure 1. Temperature-dependent ^{31}P NMR shifts of **10** in a toluene-d_8/CD_2Cl_2 (4:1) mixture.

W≡C bond vector (for more details see crystal structure discussion below), making all four phosphorus atoms inequivalent. At higher temperatures upcoming dynamic processes average the phosphorus positions within the NMR time scale, giving rise to the observed broad signal.

In contrast to **3**, complexes **10** and **11** could be oxidized in facile reactions with $[FeCp_2][PF_6]$, leading to the corresponding monocationic products **10[PF$_6$]** and **11[PF$_6$]** (Scheme 7). **10** could be oxidized further to the dicationic species **10[PF$_6$]$_2$** upon reaction with $[Ph_3C][PF_6]$. It is important to mention at this point that **11** failed the oxidation to a dicationic form, which is in constrast to **10**, where both mono- and dicationic derivatives were isolated. This confirms that only CO-free units of the type $[W(CR)(PP)_2X]$ can undergo reversible oxidation. The third diphosphine substitution forming **11** had only little effect on the ν(C≡O) position in comparison to **3**. In contrast to this, the oxidation of **11** to **11[PF$_6$]** induced a larger shift of the ν(C≡O) bands of about 15 cm^{-1} to higher energies.

Complex **10** is stable in air in solid state and only slowly decomposes in solution. It was also found that the complex is stable toward strong bases and acids such as HBF_4 and MeLi. **10** reacts with thallium triflate showing iodine substitution with the formation of thallium iodide precipitate. This reaction is currently being investigated to exploit for substitution of iodine to acetylenes.

Structural Studies of Complexes 2−8, 10, 11, 11[PF$_6$]. All compounds except **9**, **10[PF$_6$]**, and **10[PF$_6$]$_2$** were structurally characterized. The ORTEP plots of **2**, **3**, **10**, **11** are presented in Figures 2 and 3. The plots for structures of **4**−**8** and **11[PF$_6$]** are presented in the Supporting Information. Selected bond distances are summarized in Table 1.

The structure of **2** revealed a dianionic complex along with two lithium cations, which are in tetrahedral environment coordinating two THF molecules and one acetylenic bond of the C_4 bridge. The anionic part comprises two octahedral tungsten fragments, and the structure of the C_4 bridge is close to a butadiynyl form. Structures **3**, **7**, and **8** consist of a C_4 chain with pseudo-square pyramidal [*trans*-$W(CO)_2$(dppe)X] end groups (X = I (**3**), Cl (**7**), NCS (**8**)). The W−C_α bond lengths are close to the size of a triple bond.[23] The C_α−C_β bonds are longer than the central C_β−C_β', clearly indicating that the oxidation of **2** causes the structure of the C_4 bridge to transform from an acetylenic to a biscarbynic canonical form. The C_4 bridge acts as a flexible electron reservoir, which switches upon oxidation of the tungsten centers from one-electron donation (acetylenic) at each side in **2** to three-electron donation in **3**, **7**, and **8**. This indeed is the first example of related complexes to clearly document a redox-induced structural switch from an acetylene to a carbyne form of bridge. The axial ligands lead to tightening of the W≡C carbyne bonds via π donation with increasing influence from NCS to I. A related structural trend was observed in mononuclear species.[42] The π-donor effect also affects the C_α−C_β bond distances, which get longer, and the central C_β−C_β' bonds, which shorten upon going from I to NCS. The bond length alternation in the bridge (C_α−C_β vs C_β−C_γ) of **3**, **7**, **8** resembles qualitatively that of a metal-capped C_6 system.[43]

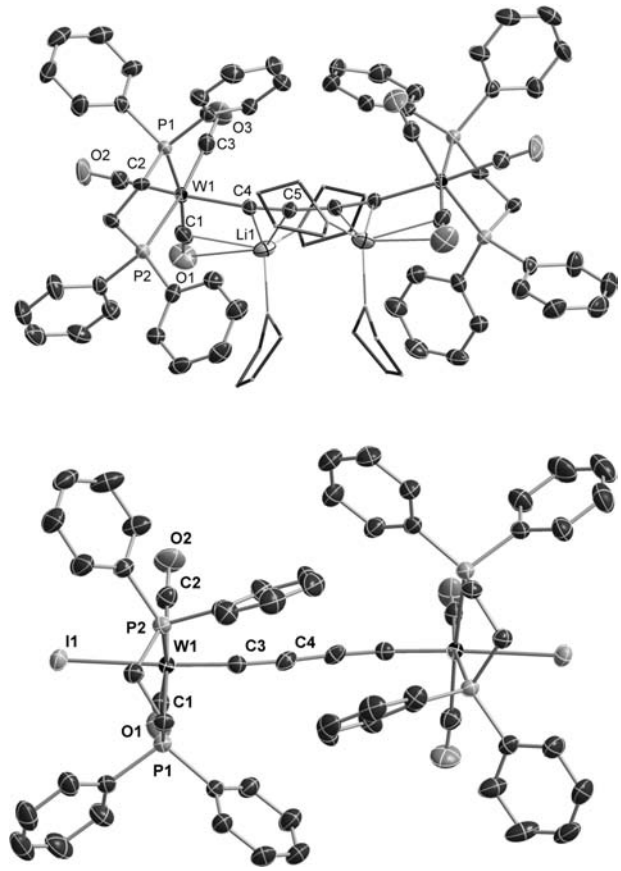

Figure 2. ORTEP-like drawing of **2** (top) and **3** (bottom) (50% probability level of thermal ellipsoids). Hydrogen atoms and solvent molecules are omitted for clarity. Coordinated THF molecules are shown in wire style.

All of the [W]C_4[W] structures display distortions from linearity. Complexes **3**, **7**, **8**, and **10** show S-shape distortion (transoid), compounds **2** and **11** have bow-shaped distortion (cisoid). For complexes containing [*trans*-$W(CO)_2$(dppe)X], the ($WC_\alpha C_\beta$) and ($C_\alpha C_\beta C_\beta'$) angles contribute approximately equally to the deviation from linearity. However, for **10** and **11** constructed from [*trans*-$W(dppe)_2X$] centers, the ($WC_\alpha C_\beta$) angles of ∼172° contribute a large portion to the total deviation more than the ($C_\alpha C_\beta C_\beta'$) angles (∼176°). Gladysz et al. have shown by DFT calculations for platinum-capped polyynes that the energetic barrier for bow-shaped distortions in [M]C_n[M] systems is quite small (about 2 kcal/mol), which is indeed in

(42) (a) Carriedo, G. A.; Riera, V.; Gonzalez, J. M. R.; Sanchez, M. G. *Acta Crystallogr., Sect. C: Cryst. Struct. Commun.* **1990**, *46*, 581–584. (b) Zhang, L.; Gamasa, M. P.; Gimeno, J.; da Silva, M. F.; C, G.; Pombeiro, A. J. L.; Graiff, C.; Lanfranchi, M.; Tiripicchio, A. *Eur. J. Inorg. Chem.* **2000**, 1707–1715.

(43) Dewhurst, R. D.; Hill, A. F.; Willis, A. C. *Organometallics* **2005**, *24*, 3043–3046.

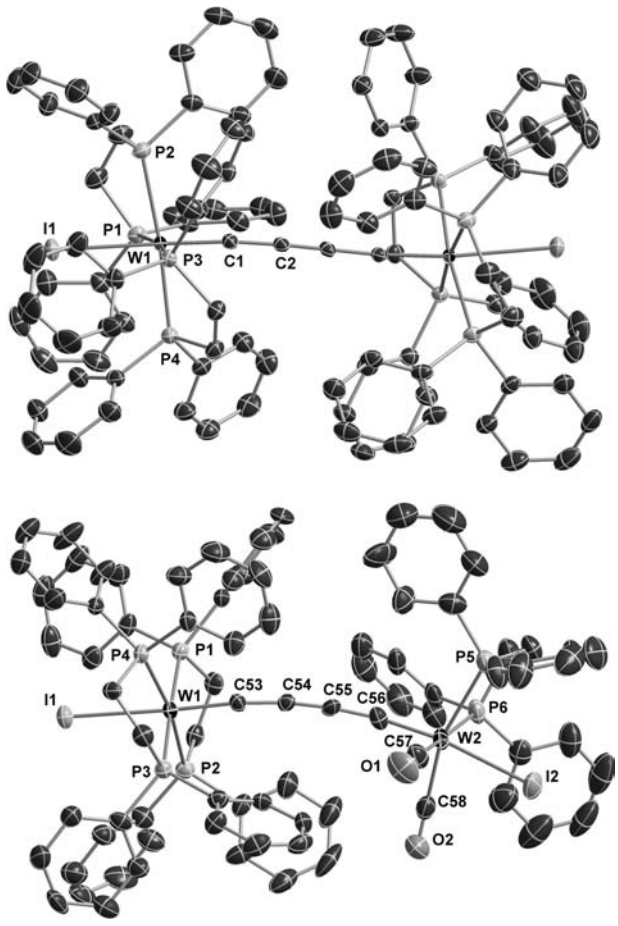

Figure 3. ORTEP-like drawing of **10** (top) and **11** (bottom) (50% probability level of thermal ellipsoids). Hydrogen atoms and solvent molecules are omitted for clarity.

Table 1. Selected Average Bond Lengths of Compounds **2**, **3**, **5**−**8**, **10**, **11**, and **11[PF$_6$]**; Assignment of the Bond Lengths in the C_4 Bridge According to the Following Notation: [W]$C_\alpha C_\beta C_\beta' C_\alpha'$[W]

bond	W−P	W−X	W−CO	W−C_α W−$C_{\alpha'}$	C_α−C_β C_α'−C_β'	C_β−C_β'
2	2.500(2)		1.987(7)	2.189(5)	1.228(8)	1.40(1)
3	2.5382(9)	2.8610(3)	2.025(4)	1.844(3)	1.320(5)	1.299(7)
5	2.514(2)	2.9121(7)	2.028(1)	1.850(9)	1.420(2)	1.38(2)
6	2.527(2)	2.519(2)	2.026	1.816(6)	1.48(2)	1.36(3)
7	2.5349(8)	2.5037(7)	2.024(3)	1.849(3)	1.346(4)	1.242(6)
8	2.533(1)	2.181(4)	2.026(5)	1.857(5)	1.352(7)	1.231(7)
10	2.4741(6)	2.8618(2)		1.847(2)	1.370(3)	1.244(4)
11	2.492(2), 2.533(2)	2.8776(6), 2.8573(7)	2.03(1)	1.849(8), 1.840(8)	1.34(1), 1.36(1)	1.27(1)
11[PF$_6$]	2.569(2), 2.525(2)	2.8291(5), 2.8500(5)	2.034(9)	1.827(6), 1.838(6)	1.359(9), 1.345(9)	1.255(9)

the range of crystal packing effects.[17,44] In accord with this observation and with the fact that **10** and **11** with bulky [*trans*-W(dppe)$_2$X] fragments are more distorted than complexes with [*trans*-W(CO)$_2$(dppe)X] units, we attribute the deviation from linearity to steric and crystal packing effects.

A comparison of **3** with **11** revealed that the "asymmetric" diphosphine substitution has only little effect on the CO bond distances of both sides. The average W−P distance at the [*trans*-W(dppe)$_2$I] center is shorter than in the [*trans*-W(CO)$_2$(dppe)X]. Also the bond alternation of the bridge is more pronounced in **3** than in **11**. The oxidized [*trans*-W(dppe)$_2$I] center of **11[PF$_6$]** shows elongated W−P bonds and a contraction of the W−I bond in comparison with the corresponding bond lengths of **11**. In general, changes of the bond lengths upon oxidation were found to be less prominent. The structural changes upon oxidation are the basis of the application of the Franck−Condon model, which would reflect the barrier for the electron transfer between the tungsten centers of dinuclear complex.

Structure **10** consists of two symmetrically arranged [*trans*-W(dppe)$_2$X] fragments bridged by a C_4 system resembling a carbynic structure [W]≡C−C≡C−C≡[W]. As previously mentioned, a comparison of **10** and **3** reveals that the W−P bonds contract upon CO substitution, and the C_4 chain shows a more pronounced [W]≡C−C≡C−C≡[W] alternation. Two important points to note for further discussion of the through-bridge metal····metal interaction for **10**: there is distortion of the [W]C_4[W] from linearity and distortion of the [*trans*-C≡W(dppe)$_2$I] fragment from C_{4v} symmetry. The S-shape of **10** is reflected by the deviation of the angle between the mean plane (P1, P2, P3, P4) and the W····W axis, which is equal to 15°. In this view the otherwise symmetrized structure of **10** would be closer to C_{2h} than to C_{4h} or D_{4d}. The coordination environment of the tungsten center is also distorted with an angle between the perpendicular of the mean plane (P1, P2, P3, P4) and the W−C axis of about 10°. Furthermore the W−P distances in **10** are significantly different, W−P3 and W−P4 (both about 2.44 Å) are shorter than the W−P1 and W−P2 distances, which are about 2.51 Å. The structural parameters of the inner coordination sphere of the tungsten centers in **5** and **6** are almost identical to those in **3** and **7** except for separations in the bridge. The W≡C bond distances reflect typical triple bond lengths. A tungsten dinuclear complex with an analogous $C_4(CH_3)_2$ bridge was structurally characterized by Templeton and co-workers.[13]

Spectroscopic Studies with Emphasis on the Characterization of the C_4 Bridges. Raman and UV−Vis Studies. Selected Raman, NMR, and UV−vis spectroscopic data are listed in Table 2. They will be discussed for the sake of a structural and electronic characterization mainly of the [W]C_4[W] unit and for the characterization of the through-bridge [W]····[W] interactions.

The Raman spectra of **3**, **6**−**11**, **10[PF$_6$]**, **10[PF$_6$]$_2$**, **11[PF$_6$]** showed strong bands around 1150 and 1930 cm^{-1} that can be attributed to the ν(WC) and symmetrical ν(C_4) vibrations, respectively (Table 2). Related carbynic structures of the complexes with substantial M≡C triple bond character were found to possess in their ν(MC) vibrations strong dependence on the nature of the carbyne substituents and only little variation with respect to the type of *trans*-carbyne ligand.[29,45] The ν(WC) vibrations of complexes **2**, **3**, **7**−**11**, **10[PF$_6$]**, **10[PF$_6$]$_2$**, **11[PF$_6$]** appear at significantly lower wavenumbers than those of mononuclear complexes of the type [(X)(CO)$_2$(dppe)W≡C−R] (∼1300 cm^{-1}) indicating electronic delocalization presumably with contribution from the carbenic form of the bridge. Similarly, ν(CC) bands of these compounds were observed around 1930 cm^{-1} at significantly lower energies than ν(C≡C) vibrations of related mononuclear tungsten carbyne complexes in conjugation with C≡C bonds.[31] Those modes were observed in the range of 2050−2100 cm^{-1}. For the dinuclear [{Cp*(PPh$_3$)(NO)Re}$_2$(μ-C_4)] complex, the ν(C_4) vibration was located at 2056 cm^{-1}. The strong shifts of the ν(C_4) Raman bands of complexes **2**, **3**, **7**−**11**, **10[PF$_6$]**, **10[PF$_6$]$_2$**, **11[PF$_6$]** also indicate

(44) Szafert, S.; Gladysz, J. A. *Chem. Rev.* **2003**, *103*, 4175–4206.

(45) Dao, N. Q. *J. Organomet. Chem.* **2003**, *684*, 82–90.

Table 2. Raman, NMR and UV−Vis Data of Complexes **2**, **3**, **5**-**11**, **10[PF$_6$]**, **10[PF$_6$]$_2$** and **11[PF$_6$]**

	Raman [cm^{-1}]		NMR [ppm]			absorption [nm]	
	ν(C$_4$)	ν(WC)	^{31}P{^{1}H} ($^1J_{W-P}$ (d, satellite) [Hz])	^{13}C (C$_\alpha$ (C$_\alpha$′))	^{13}C (C$_\beta$ (C$_\beta$′))	λ_1 (ε/1000 [M^{-1} cm^{-1}])	λ_2[a] (ε/1000 [M^{-1} cm^{-1}])
2[b]	2080		34.4 (202)	106.2	106.9	274 (45)	460 (3.2)
3	1947	1149, 1109	29.3 (228)	225.2	87.5	407 (340)	533 (5.6)
5[b,c]	1474	1067	28.0 (225)			462 (39)	
6[b,c]			38.2 (230)			450 (30)	
7	1936	1149, 1113	37.5 (226)	228.4	85.8	382 (190)	517 (3)
8	1923	1114, 1082	39.9 (234)	232.1	82.1	412 (330)	543 (4.7)
9	1964	1173, 1127	44.8 (236)		82.1	367 (400)	524 (2.5)
10	1892	1084	45	213.1	86.5	412 (290)	668 (2.3)
10[PF$_6$]	1894	1082				410 (300)	702 (1.8), 470 (6)
10[PF$_6$]$_2$	1895	1078				413 (160)	520 (7.8), 660 (1.7)
11[d]	1916	1141, 1100	38.7 (230), (32.3) (268)	230.3 (212.3)	93.9 (83.0)	416 (300)	780 (1), 480 (4.5)
11[PF$_6$]	1936	1143, 1096				406 (280)	503 (7), 620 (2.7)

[a] For the unsymmetrical complexes two absorptions of lower intensity are present. [b] **2**, **5**, **6** have an electronic structure deviating from those of the other compounds; therefore, the classification of the UV−vis absorption bands differs from those of the other complexes. [c] In the first column ν(C═C). [d] The NMR chemical shifts in brackets belong to the [(I)(dppe)$_2$W≡C−] fragment.

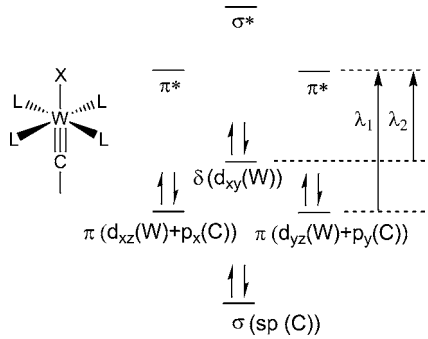

Figure 4. Qualitative molecular orbital diagram for a tungsten carbyne complex of the type discussed.

reduced bond orders in agreement with contribution from the biscarbenic form of [W]C$_4$[W] π-system.

It should be mentioned at this point that differences of the ancillary ligand sphere of complexes **3** and **7**−**12** also influence the ν(C$_4$) Raman bands. For instance, the triflate derivative **9** shows a high-energy shift of the ν(C$_4$) vibration by about 30 cm^{-1}, the dppe-substituted complex **10** shows significant shifts (30−100 cm^{-1}) of both ν(C$_4$) and ν(WC) to lower energies with respect to the corresponding band of **3**.

The UV−vis spectra of the symmetrical complexes **3**, **7**−**10** show two main absorptions λ_1 and λ_2. The best approximation for the electronic description of the [W]C$_4$[W] systems is a formulation with the bridge in the carbynic form (Figure 4).[28]

Indeed for the complexes described in this paper, two electronic transitions were found with one quite intense absorption at about 400 nm assigned to a $\pi \rightarrow \pi^*$ (λ_1) transition, while the weaker absorption is anticipated to be associated with a $d_{xy} \rightarrow \pi^*$ (λ_2) transition. Figure 4 comprises a qualitative MO scheme showing that the position of λ_1 should be in a first-order approximation affected only by the axial ligands, while λ_2 is mainly influenced by the equatorial ligands due to changes in the energy of the d_{xy} orbital being of δ-type with ideally no or only little orbital interaction with the bridge π-orbitals. The experiments confirmed the qualitative picture of Figure 4. The position of the $\pi \rightarrow \pi^*$ (λ_1) transition is indeed changing with the axial ligand X, as observed for complexes **3**, **7**−**9**. However, significant changes in the equatorial ligand patterns on going from **3** to **10** did not influence λ_1 but strongly shifted λ_2 from 533 to 668 nm. The decreasing energy of λ_2 is in agreement with a decrease in the π-acceptor properties of the dppe relative to the CO ligand resulting in an energetic increase of d_{xy}. The spectra of the unsymmetrical complexes **11**, **11[PF$_6$]**, **10[PF$_6$]** show one strong and two weak absorptions.

Electronic Communication between the Tungsten Centers. The interaction between the metal centers in the [W]C$_4$[W] systems was evaluated on the basis of the stabilization energy of the mixed-valence complex, electronic delocalization, electron-transfer capability, and ordering in the spin system.[3−5,46−48]

CV Evidence for Stabilization of Mixed-Valence Complexes. As expected, the unsymmetrical complex **11** has only one reversible redox step with an $E_{1/2}$ value of −435 mV *vs* Fc$^{0/+}$ (Figure 5). This is explained on the basis that only the pure phosphine-substituted tungsten center has reversible redox properties. The unpaired electron is therefore expected to be localized in the d_{xy} orbital of the [(I)(dppe)$_2$WC−] unit.[49−51] The given $E_{1/2}$ value is, however, found at significantly higher potential than those of the mononuclear carbyne complexes ([ClW(dmpe)$_2$(CH)] −880 mV and [ClW(PMe$_3$)$_4$(CH)] −910 mV), indicating direct influence of the P_4 framework in-plane with the HOMO of such systems (Figure 4). This lower reduction potential is assumed to be due to lower σ-donating and higher π-accepting properties of the dppe ligand. For the symmetric complex **10** two oxidation waves were found at −543 mV and −253 mV revealing that both tungsten centers are involved in the redox process. But a relatively small peak separation of **10** was observed witnessing only moderate electronic coupling of the tungsten centers.

Under rigorous symmetry conditions, i.e. molecular distortions or pseudo-symmetries excluded, the HOMO is of δ-type

(46) Astruc, D. *Acc. Chem. Res.* **1997**, *30*, 383–391.
(47) McCleverty, J. A.; Ward, M. D. *Acc. Chem. Res.* **1998**, *31*, 842–851.
(48) Barlow, S.; O'Hare, D. *Chem. Rev.* **1997**, *97*, 637–669.
(49) Salaymeh, F.; Berhane, S.; Yusof, R.; de la Rosa, R.; Fung, E. Y.; Matamoros, R.; Lau, K. W.; Zheng, Q.; Kober, E. M.; Curtis, J. C. *Inorg. Chem.* **1993**, *32*, 3895–3908.
(50) Richardson, D. E.; Taube, H. *Coord. Chem. Rev.* **1984**, *60*, 107–129.
(51) (a) Gagne, R. R.; Spiro, C. L.; Smith, T. J.; Hamann, C. A.; Thies, W. R.; Shiemke, A. D. *J. Am. Chem. Soc.* **1981**, *103*, 4073–4081. (b) Moore, K. J.; Lee, L.; Mabbott, G. A.; Petersen, J. D. *Inorg. Chem.* **1983**, *22*, 1108–1112.

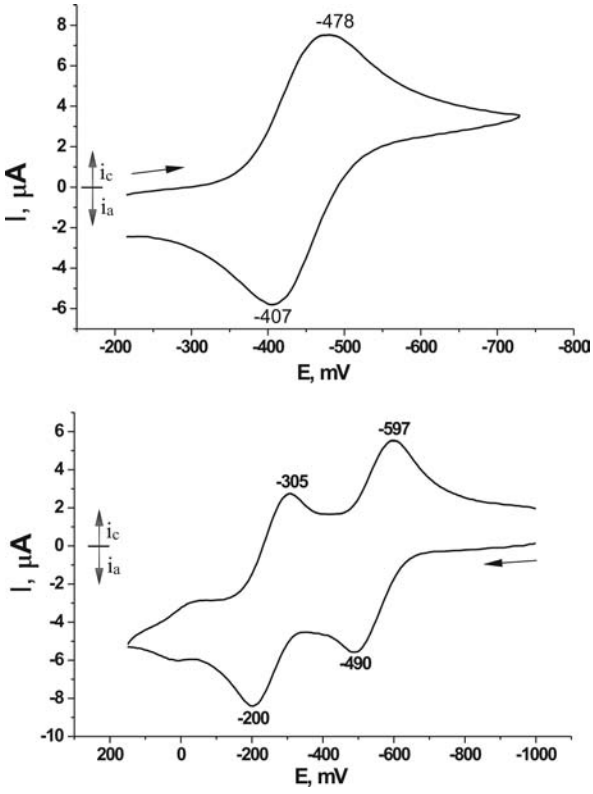

Figure 5. Cyclic voltammogram for **11[PF$_6$]** (top) and **10** (bottom) in CH_2Cl_2 with 0.1 M [nBu$_4$N][PF$_6$]; Au electrode; E vs $Fc^{0/+}$; scan rate = 100 mV/s; 20 °C.

(Figure 4) not allowing interactions with the halogens or the bridge system, which possess σ- or π-type orbitals. Due to this, orbital overlap between the HOMO or SOMO and the bridge can not occur. In a C_{4h} or D_{4d} structure this would prevent π-orbital influence of the axial ligands on the redox properties of such species.[41] Nevertheless a through-bridge electronic coupling was observed, which is thought to originate from symmetry lowering allowing with just "approximate" orthogonality of the π-type orbitals of the bridge and the *axial* ligands with the HOMO or SOMO of δ-type symmetry. As we have seen, a symmetry lowering to C_{2h} in the solid-state structure of **10** is evident. It is also prevailing in solution as confirmed by ^{31}P NMR. Symmetry lowering induces mixing of the δ-orbital with the d_{xz} and d_{yz} orbitals and consequently electronic communication depending on the extent of the mixing. A spin−orbital coupling may be another important factor for tungsten contributing mixing between orbitals of different symmetry.

The ΔE value for **10** of 290 mV ($K_c = 7.5 \times 10^4$) is similar to that reported for another related C_4-bridged system with low-symmetry end groups (250 mV).[33] It is indicative of a borderline class II-/III-type system according to the Robin−Day classification.[52] The peak separation is also solvent dependent, since in THF a ΔE value of 250 mV was found (see Supporting Information). Another explanation for this small but significant peak splitting was reported in the literature.[49] In accordance with this, the oxidation of the [M]C_4[M] system would lead to enhancement of the π-acceptor properties of the C_4 chain to stabilize the system and consequently to increase the second oxidation potential.

(52) Robin, M. B.; Day, P. *Adv. Inorg. Chem. Radiochem.* **1967**, *10*, 247–422.

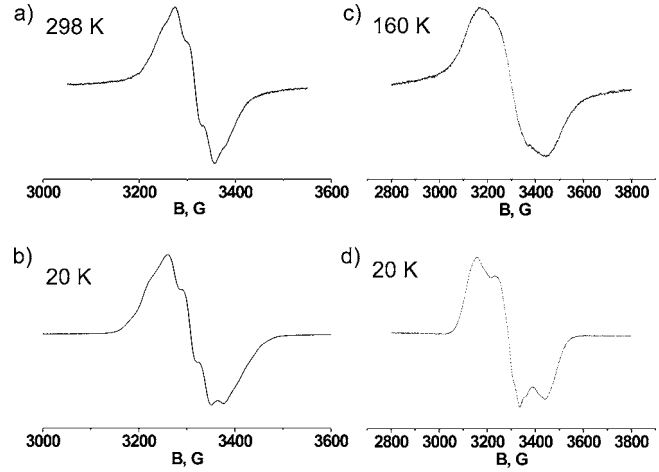

Figure 6. EPR spectra of (a) **11[PF$_6$]** at 298 K in CH_2Cl_2 solution; (b) **11[PF$_6$]** at 20 K in CH_2Cl_2 glass; (c) **10[BAr$^f_4$]** at 160 K in toluene solution; (d) **10[PF$_6$]** at 20 K in CH_2Cl_2/toluene glass.

EPR Study for Through-Bridge Electron Transfer in the Dinuclear Complexes. Localization or delocalization of an electron becomes evident through signal averaging at metal centers using different methods, such as EPR and IR.[3,5] Therefore, EPR measurements were carried out for **11[PF$_6$]**, **10[PF$_6$]**, **10[BAr$^f_4$]**, and **10[PF$_6$]$_2$** (Figure 6). **10[BAr$^f_4$]** (BAr$^f_4$-tetrakis[(3,5-trifluoromethyl)phenyl]borate) was used instead of **10[PF$_6$]** due to its solubility in toluene, which was required as a solvent to obtain a good signal-to-noise ratio in 100−200 K temperature interval. Compound **10[BAr$^f_4$]** was prepared *in situ* by anion exchange between Na[BAr$^f_4$] and **10[PF$_6$]**. The EPR spectra of **10[PF$_6$]** and **10[BAr$^f_4$]** in frozen CH_2Cl_2 at 20 K are completely identical. No clear signal was detected for **10[PF$_6$]$_2$**, apparently due to strong antiferromagnetic interactions.

Compound **11[PF$_6$]** showed one signal with $g = 2$ at room temperature and in frozen toluene solution, confirming electron localization on the [*trans*-W(dppe)$_2$I] center. The signal is fully symmetrical at room temperature and revealed only slight asymmetry in glass, which reflects only small spin−orbit coupling as expected from the molecular orbital diagram with the unpaired electron localized in the energetically rather isolated d_{xy} orbital (see Figure 4). A hyperfine coupling is detected due to coupling with the four phosphorus nuclei. Thus, the solution spectra of **11[PF$_6$]** could be modeled with a hyperfine ^{31}P coupling constant of 31 G and a line broadness of 20 G. The EPR spectrum of the mixed-valence complex **10[PF$_6$]** did not show any signal at room temperature. A signal of reasonable intensity was observed only below 160 K. The line broadness was then almost twice that of the signal of **11[PF$_6$]** which prevented observation of hyperfine coupling. The spectrum in frozen toluene solution at 20 K showed stronger anisotropy than in the case of **11[PF$_6$]**.

The broadness of the signal of **10[PF$_6$]** is interpreted in terms of electron dynamics with intramolecular transfer between the remote metal ends or with a stronger spin−orbit coupling.

IR Investigation of Through-Bridge Electron Transfer in the Dinuclear Complexes. IR can usually be utilized as a probe to measure the extent of the electron delocalization via the extent of averaging of the characteristic absorptions strongly affected by the oxidation state of the metal center. Furthermore, in symmetry-lowered systems with electron exchanges between the metal centers slow on the IR time scale (10^{-13} s), one can often identify new absorptions forbidden to appear in a

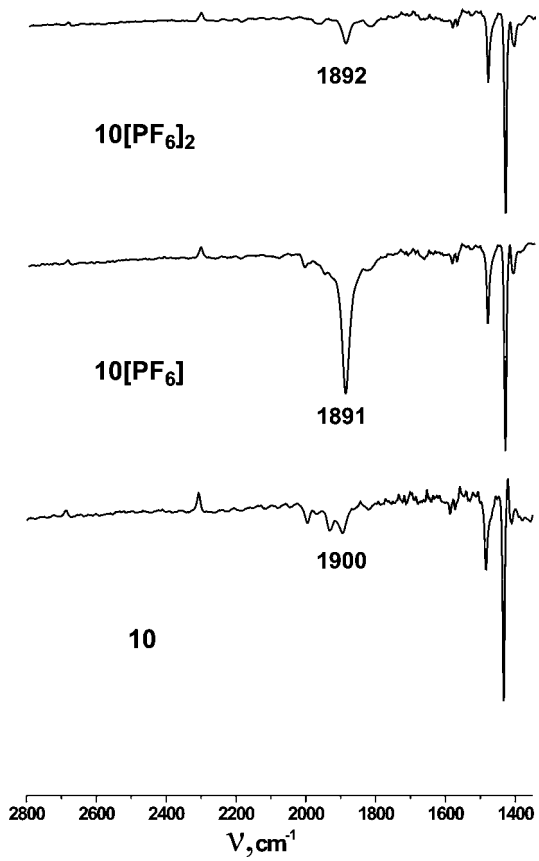

Figure 7. $\nu(C_4)$ absorptions in the IR spectra of **10**, **10[PF$_6$]**, and **10[PF$_6$]$_2$** (CH_2Cl_2, room temperature, 5×10^{-3} M).

symmetrical system.[3,53] In the spectra of the mixed-valence complex we did not find shifts for any absorption that might originate from oxidation of the metal center; however, our system seemed to be well suited for the latter approach, because of the highly symmetric C_4 bridge and the IR forbidden central ν(CC) vibration. The appearance of an intense ν(CC) band in the IR spectrum of **10[PF$_6$]** indicates that this vibration is no longer forbidden, because on the IR time scale the centered symmetry of the molecule is apparently broken by tungsten centers of different electron counts. The IR spectra of the complexes **10**, **10[PF$_6$]** and **10[PF$_6$]$_2$** are presented in Figure 7.

The IR spectra of the symmetrical complexes **10** and **10[PF$_6$]$_2$** are presented for comparison in Figure 7 demonstrating the presence of only weak $\nu(C_4)$ bands. In contrast to **10** and **10[PF$_6$]$_2$**, **10[PF$_6$]** possesses an intense band at 1981 cm^{-1} corresponding to a symmetric $\nu(C_4)$ vibration. As mentioned previously, the presence of strong symmetrical ν(CC) vibration is an indicator of localization in the IR time scale. It should be mentioned that delocalization in such a short time regime would be characteristic of full delocalization and typically observed only for strongly interacting systems.[48]

NIR Evidence for Through-Bridge Electron Transfer in the Dinuclear Complexes. The electron transfer between the metal centers is sketched in the schematic energy diagram in Figure 8.[2]

Near-IR spectroscopy allows direct measurement of the reorganization parameter λ and approximation of the electronic coupling energy H_{ab} via the following equations:[3]

$$H_{ab}(cm^{-1}) = [(4.2 \times 10^{-4})\varepsilon\Delta\bar{\nu}_{1/2}E_{IT}]^{1/2}/d;\ \lambda = E_{IT}$$

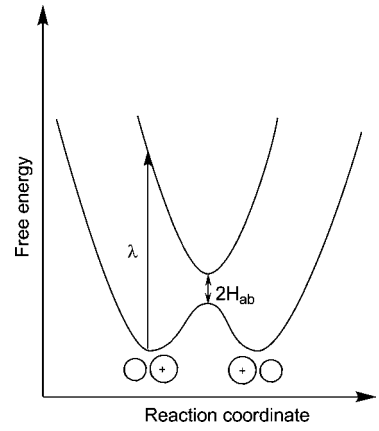

Figure 8. Schematic energy diagram explaining the origin of the charge transfer bands in the near-IR range.

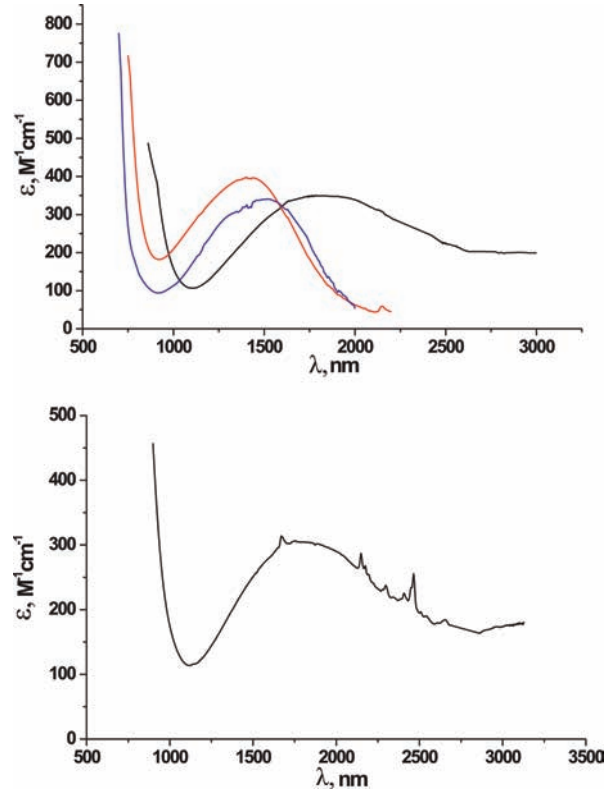

Figure 9. NIR spectra for **10[PF$_6$]** (black), **11[PF$_6$]** (blue), and **10[PF$_6$]$_2$** (red) in CH_2Cl_2. Regions with high noise due to solvent absorptions were linearly approximated. The bottom spectrum shows the NIR absorption of **10[PF$_6$]** in $CDCl_3$, where the solvent background is less than that in CH_2Cl_2.

where ε is the absorption coefficient in M^{-1} cm^{-1}, $\Delta\nu_{1/2}$ the width of the absorption band at half-height in cm^{-1}, E_{IT} the energy of the band maximum in cm^{-1}, and d the electron transfer distance in Å. The spectra for **11[PF$_6$]**, **10[PF$_6$]**, and **10[PF$_6$]** are presented in Figure 9.

All spectra are of relatively low intensity and broad especially that of **10[PF$_6$]**. The bands of **11[PF$_6$]** and **10[PF$_6$]$_2$** are centered at significantly higher energies than those of **10[PF$_6$]**. The fact that **11[PF$_6$]** and **10[PF$_6$]$_2$** have a similar absorption in the NIR supports the idea that this absorption is a result of a $\pi \rightarrow d_{xy}$ transition (see Figure 4). The spectrum of **10[PF$_6$]** can be explained as a superposition of a $\pi \rightarrow d_{xy}$ transition and a charge-transfer transition, Figure 9. Calculations with overlapping bands

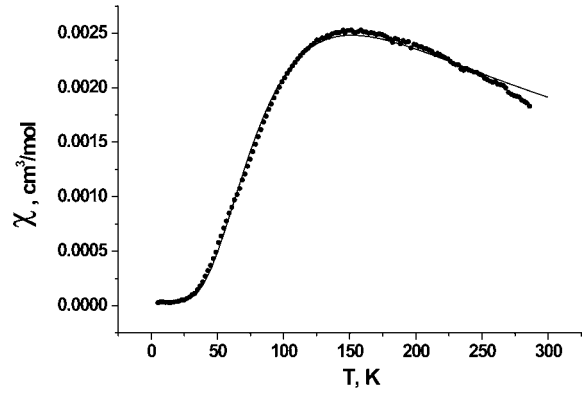

Figure 10. Temperature dependence of χ vs T for **10[PF$_6$]$_2$**. The data are corrected for core diamagnetism, van Vleck paramagnetism, and other temperature-independent contributions. Contribution from a small (on the level of 2%) paramagnetic impurity has been compensated. The uncorrected data are presented in the Supporting Information.

must possess tentative character. We estimated by using the right edge of the plateau of the given band as the center of the charge transfer band in the calculations. An estimate of the reorganization parameter λ for **10[PF$_6$]** from this absorption band amounts to 2000 nm (5000 cm^{-1}). This value is significantly smaller in energy than those of the majority of published systems detected in the range of 1000 to 1500 nm.[3,48,50,54] The low value would indicate a small reorganization energy, which is in agreement with the derived structural data, where only small changes in bond distances were detected upon oxidation. Approximation of H_{ab} leads to an energy of about 250 cm^{-1}. Within the nonadiabatic limit, the rate constant for electron transfer is given by the following equation:[2,55]

$$k = (2H_{ab}^2/\hbar)(\pi^3/\lambda k_b T)^{1/2}\exp(-\lambda(1 - 2H_{ab}/\lambda)^2/4k_b T)$$

From this equation we calculated a value of 1.5×10^{11} s^{-1} for our system, which is consistent with electron localization on the IR time scale and with a borderline case between localized behavior and an averaging situation for the EPR exchange.

Magnetic Measurements to Characterize Through-Bridge Electronic Interaction in the Dinuclear Complexes. The magnetic properties of **11[PF$_6$]**, **10[PF$_6$]**, and **10[PF$_6$]$_2$** were established by variable-temperature magnetization measurements. The magnetic susceptibilities of **11[PF$_6$]** and **10[PF$_6$]** showed a typical paramagnetic behavior, as could be expected from the presence of one unpaired electron in these molecules (Figures 8S and 9S in the Supporting Information). The magnetic susceptibility of **10[PF$_6$]$_2$** shows a maximum at 150 K (Neel temperature) and drops considerably on going to higher temperatures (Figure 10).

Thus, the magnetic behavior of **10[PF$_6$]$_2$** is typical of a strongly antiferromagnetically coupled spin dimer. To obtain an estimate of the exchange coupling, we fitted the experimental data with the equation for a spin-$^1/_2$ dimer model (spin Hamiltonian: $H = -J\mathbf{S_1}\cdot\mathbf{S_2}$):

$$\chi = \frac{2N_A g^2\beta^2}{kT}\cdot\frac{1}{(3 + e^{J/kT})}$$

with g and J as parameters. The minimized value for the g-factor is close to a free electron value of 2. The derived J indicates a singlet−triplet gap equal to 167 cm^{-1}, which is significantly more than 26 cm^{-1} observed for related bis-carbyne complex and than J for dinuclear W and Mo complexes in low spin d^5 and d^1 configurations.[47,56,57] Comparable values of exchange energies were obtained for dinuclear ruthenium complexes.[58] The antiferromagnetic nature of the spin interactions could be explained by a spin-polarization mechanism involving eight p-orbitals of the bridge.[57] The presence of strong antiferromagnetic coupling provides additional evidence for the interaction of metal orbitals with the π-orbitals of the bridge required for the mediation of magnetic ordering over long distance. The original data showed also presence of small paramagnetic impurities. The amount of these impurities was estimated using a fitting procedure of the sum of the antiferromagnetic and paramagnetic contributions on the level of 2% (see Supporting Information for details). This paramagnetic contribution was subtracted from the presented curve.

Conclusion

A versatile synthetic route to C_4-bridged tungsten complexes of the type [W]C_4[W] ([W] = [(X)W(dppe)(CO)$_2$] and [(X)W(dppe)$_2$]) was developed. The structures of the W(0) complexes were found to be close to a diacetylenic canonical form [W(0)]−C≡C−C≡C−[W(0)], while the structures with W(II) centers could be ascribed with biscarbynic bridge structures [W(II)]≡C−C≡C−C≡[W(II)]. The termini could be functionalized with reactive triflate substituents to eventually enable expansion of these dinuclear systems to polynuclear complexes. The mixed-valent complex **10[PF$_6$]** was found to reflect a class II system of the Robin−Day classification[52] possessing medium M····M "electronic communication" with barrier between the remote metal termini. The rate of electron transfer in this system was found to be in the same range as the EPR time scale, but appeared localized on the IR time scale. The remarkable stability, along with the ease of functionalization of the metal termini makes these complexes suitable candidates for "with barrier" organometallic wires to build complex single-electron devices.

Experimental Section

General Procedures. All the manipulations were carried out under a nitrogen atmosphere using Schlenk techniques or a drybox. Reagent grade benzene, toluene, hexane, pentane, diethyl ether, and tetrahydrofuran were dried and distilled from sodium benzophenone ketyl prior to use. Dichloromethane and acetonitrile were distilled from CaH_2, and chloroform was dried by P_2O_5. The modified literature procedures were used to prepare the following compounds: W(CO)$_3$(dppe)(THF),[35] Li_2C_4(THF)$_x$,[36] see Supporting Information

(53) Demadis, K. D.; El-Samanody, E. S.; Coia, G. M.; Meyer, T. J. *J. Am. Chem. Soc.* **1999**, *121*, 535–544.
(54) Ward, M. D. *Chem. Soc. Rev.* **1995**, 121–134.
(55) Sutin, N. *Prog. Inorg. Chem.* **1983**, *30*, 441–498.
(56) (a) Hu, J. S.; Sun, J. B.; Hopkins, M. D.; Rosenbaum, T. F. *J. Phys.: Condens. Matter* **2006**, *18*, 10837–10841. (b) Thompson, A. M. W. C.; Gatteschi, D.; McCleverty, J. A.; Navas, J. A.; Rentschler, E.; Ward, M. D. *Inorg. Chem.* **1996**, *35*, 2701–2703. (c) Stobie, K. M.; Bell, Z. R.; Munhoven, T. W.; Maher, P. J.; McCleverty, J. A.; Ward, M. D.; McInnes, E. J. L.; Totti, F.; Gatteschi, D. *Dalton Trans.* **2003**, 36–45.
(57) Ung, V. A.; Thompson, A. M. W. C.; Bardwell, D. A.; Gatteschi, D.; Jeffery, J. C.; McCleverty, J. A.; Totti, F.; Ward, M. D. *Inorg. Chem.* **1997**, *36*, 3447–3454.
(58) Aquino, M. A. S.; Lee, F. L.; Gabe, E. J.; Bensimon, C.; Greedan, J. E.; Crutchley, R. J. *J. Am. Chem. Soc.* **1992**, *114*, 5130–5140.

for details. All other chemicals were used as obtained from commercial suppliers. IR spectra were obtained on a Bio-Rad FTS-45 instrument and Bio-Rad Excalibur FTS-3500. NMR spectra were measured on a Varian Mercury spectrometer at 200 MHz for ^{1}H and 81 MHz for ^{31}P{^{1}H}, Varian Gemini-2000 spectrometer at 300 MHz for ^{1}H and 75 MHz for ^{13}C{^{1}H} and on a Bruker-DRX-500 spectrometer at 500 MHz for ^{1}H, 125.8 MHz for ^{13}C{^{1}H} and 202.5 MHz for ^{31}P{^{1}H}. Chemical shifts for ^{1}H and ^{13}C are given in ppm relative to TMS and those for ^{31}P relative to phosphoric acid. The UV−vis and near-IR spectra were recorded on a Varian CARY 50 Scan UV−visible and on a Varian CARY 500 Scan UV−visible−near-IR spectrometers. CHN elemental analyses were performed with a LECO CHN-932 microanalyzer. Raman spectra were recorded on a Renishaw Ramanscope spectrometer (633 nm). Cyclic voltammograms were obtained with BAS 100W voltammetric analyzer equipped with the low volume cell. The cell was equipped with an Au working and a Pt counter electrode, and a non-aqueous reference electrode. All sample solutions (CH_2Cl_2) were approximately 5×10^{-3} M in substrate and 0.1 M in Bu_4NPF_6, and were prepared under nitrogen. Ferrocene was subsequently added and the calibration of voltammograms recorded. BAS 100W program was employed for data analysis. X-band EPR spectra were obtained using Bruker EMX Electron Spin Resonance system. To measure spectrum of $\mathbf{10}^+$ at different temperatures toluene solution was required. Due to insolubility of **10[PF$_6$]** in toluene, the **[PF$_6$]**$^-$ counter-ion was exchanged to **[BAr$^f_4$]**$^-$ by treatment of **10[PF$_6$]** with Na[BAr$^f_4$] in CH_2Cl_2. The spectra of **10[PF$_6$]** and **10[BAr$^f_4$]** in frozen solution at 20 K are fully identical. A solution spectrum of **11[PF$_6$]** was modeled with help of Bruker WIN EPR Simfonia software. Magnetization measurements were carried out on a Quantum Design SQUID magnetometer, molar magnetic susceptibility was calculated according to the equation $\chi = (M \cdot M_w)/(m \cdot H)$, where M = experimental magnetization, M_w = molecular weight, m = sample weight, H = magnetic field.

X-ray Diffraction Studies on 2−8, 10, 11, 11[PF$_6$]. Data collection for crystals of **2** and **6**, were carried out on Stoe IPDS diffractometer (Imaging Plate Detector System with graphite-monochromated Mo K_α radiation, $\lambda = 0.71073$ Å)[59] and for others on Oxford Diffraction Xcalibur R diffractometer (4-circle kappa platform, Ruby CCD detector and a single wavelength Enhance X-ray source with Mo K_α radiation, $\lambda = 0.71073$ Å) at 183(2) K using a cold N_2-gas stream from an Oxford Cryogenic System. Pre-experiment, data collection, and data reduction (unit cell determination, intensity data integration, and empirical absorption correction) for for **3**−**8**, **10**, **11**, **11[PF$_6$]**: were carried out with the Oxford *CrysAlisPro* software.[60] The structures were solved with the unique data sets using the Patterson method of the program SHELXS-97. The structure refinement was performed with the program SHELXL-97.[61] Non-hydrogen atoms were refined anisotropically by full-matrix least-squares techniques based on F^2. The hydrogen atoms of the organic groups were placed in calculated positions and refined with a riding model with a fixed temperature factor. The program PLATON[62] was used to check the result of the X-ray analysis. The disorders observed for one THF molecule in **1**, for the positions of the $-CH_2-CH_2-$ units of the dppe ligand and for the C_4 bridge between the transition metals in **7** and **8**, were treated with the EADP and PART instructions of SHELXL-97 and anisotropically refined. Further details on all structures are provided in Tables 1Sa and 1Sb, and in the form of cif files available as part of the Supporting Information or from the CCDC under deposition numbers 754637−754645 and 755094.

Li$_2$[(CO)$_3$(dppe)WC$_4$W(CO)$_3$(dppe)] (THF)$_3$(C$_6$H$_6$)$_2$ (2). Solid $Li_2C_4(THF)_x$ (150 mg) was added to a solution of $W(CO)_3$(dppe)(THF) (1 g, 1.35 mmol) in 80 mL of THF. This mixture was stirred during 18 h at 55 °C. The resulting brown suspension was filtered and concentrated to 20 mL *in vacuo*. Complex **2** was obtained as a powder after addition of benzene (60 mL) to the THF solution. The product was recrystallized from a glyme/ether mixture. Yield: 610 mg (0.346 mmol, 51%). Single crystals suitable for X-ray diffraction were grown by addition of ether to the THF solution of **2**. Anal. Calcd for $C_{86}H_{84}Li_2O_9P_4W_2$: C, 58.45; H, 4.79. Found: C, 58.24; H, 4.69. IR (cm^{-1}): 2050 (C≡C), 1892 (CO), 1814 (CO), 1726 (CO). ^{1}H NMR (200 MHz, THF-d_8) δ = 7.99−7.71 (m, 15H, C_6H_5), 7.38−7.22 (m, 25H, C_6H_5), 2.83 (m, 4H, CH_2), 2.35 (m 4H, CH_2). ^{31}P NMR (81 MHz, THF-d_8) δ = 34.40 (s, $^1J_{W-P}$ (d, satellite) = 202 Hz). ^{13}C NMR (125 MHz, THF-d_8) δ = 218.5 (dd, $^2J_{C-P(cis)}$ = 7.3 Hz, $^2J_{C-P(trans)}$ = 34.5 Hz, CO (equatorial)), 213.5 (s, CO (axial)), 140.7 (d, $^1J_{C-P}$ = 37.5 Hz, *ipso*-C_6H_5), 140.0 (d, $^1J_{C-P}$ = 37.5 Hz, *ipso*-C_6H_5), 129.2 (s, C_6H_5), 128.7 (s, C_6H_5), 128.1 (m, C_6H_5), 106.9 (s, C_β), 106.2 (t, $^2J_{C-P}$ = 12.5 Hz, C_α), 32.3 (dd, $^1J_{C-P}$ = 18.5 Hz, $^2J_{C-P}$ = 18.0 Hz, CH_2).

[I(CO)$_2$(dppe)WC$_4$W(CO)$_2$(dppe)I] (3). Ten milliliters of a THF solution of iodine (121 mg, 0.47 mmol) was added dropwise to a solution of **2** (400 mg, 0.23 mmol) in glyme/THF (10/15 mL) at −60 °C. After stirring the reaction mixture for 20 min, the cooling bath was removed, and the mixture was additionally stirred for 6 h at room temperature. The resulting brown-violet solution was evaporated to dryness *in vacuo*. Addition of acetonitrile (5 mL) resulted in the formation of violet crystals of **3** (300 mg, 0.19 mmol) which were filtered and washed with acetonitrile (10 mL). A second crystallization from the filtrate afforded an additional 30 mg (0.019 mmol) of the desired product **3**. Yield: 330 mg (0.21 mmol, 91%). Single crystals suitable for X-ray diffraction were grown by cooling a dichloromethane solution of **3**. Anal. Calcd for $C_{60}H_{48}I_2O_4P_4W_2$: C, 45.66; H, 3.07. Found: C, 45.76; H, 3.20. IR (cm^{-1}): 1990 (CO), 1929 (CO). ^{1}H NMR (500 MHz, CD_2Cl_2) δ = 7.68−7.58 (m, 16H, C_6H_5), 7.46−7.42 (m, 8H, C_6H_5) 7.41−7.37 (m, 4H, C_6H_5), 7.27−7.23 (m, 4H, C_6H_5), 7.18−7.13 (m, 8H, C_6H_5), 3.1 (m, 4H, CH_2), 2.6 (m, 4H, CH_2). ^{31}P NMR (81 MHz, CD_2Cl_2) δ = 29.32 (s, $^1J_{W-P}$ (d, satellite) = 228 Hz). ^{13}C NMR (125 MHz, CD_2Cl_2) δ = 225.2 (t, $^2J_{C-P}$ = 11.1 Hz, C_α), 211.2 (dd, $^2J_{C-P(cis)}$ = 6.9 Hz, $^2J_{C-P(trans)}$ = 43,0 Hz, CO), 134.7 (d, $^1J_{C-P}$ = 25.1 Hz, *ipso*-C_6H_5), 134.3 (d, $^1J_{C-P}$ = 25.2 Hz, *ipso*-C_6H_5), 133.3 (d, $^2J_{C-P}$ = 11.9 Hz, *ortho*-C_6H_5), 132.5 (d, $^2J_{C-P}$ = 9.8 Hz, *ortho*-C_6H_5), 130.7 (d, $^4J_{C-P}$ = 62.5 Hz, *para*-C_6H_5), 128.7 (t, $^3J_{C-P}$ = 10.5 Hz, *meta*-C_6H_5), 87.5 (t, $^3J_{C-P}$ = 3.7 Hz, C_β) 38.4 (dd, $^1J_{C-P}$ = 28.1 Hz, $^2J_{C-P}$ = 11.9 Hz, CH_2).

[IW(CO)$_3$(dppe)(CCPh)] (4). A solution of lithium phenylacetylide (7.5 mg, 0.068 mmol) in THF (2 mL) was slowly added to a solution of $W(CO)_3$(dppe)(THF) (60 mg, 0.068 mmol) in 5 mL of THF. This mixture was stirred during 20 min at room temperature. To the resulting yellow solution of Li[$W(CO)_3$(dppe)(CCPh)] was added dropwise a THF solution of iodine (17 mg, 0.068 mmol) at −20 °C. The resulting brown-yellow solution was evaporated to dryness *in vacuo*. Addition of acetonitrile (2 mL) to the remaining solid led to the formation of orange crystals of **4**, which were filtered and washed with acetonitrile (5 mL). Single crystals suitable for X-ray diffraction were grown by layering a CH_2Cl_2 solution with acetonitrile. Yield: 38 mg (0.043 mmol, 63%). Anal. Calcd for $C_{37}H_{29}IO_3P_2W$: C, 49.58; H, 3.49. Found: C, 49.50; H, 3.41. IR (cm^{-1}): 2024 (CO), 1955 (CO), 1896 (CO). ^{1}H NMR (200 MHz, CD_2Cl_2) δ = 7.67 (br, 15H, PC_6H_5), 7.46 (m, 25H, PC_6H_5), 7.04 (m, 3H, CCC_6H_5), 6.55 (m, 2H, CCC_6H_5), 2.85−2.65 (m, 4H, CH_2). ^{31}P NMR (81 MHz, CD_2Cl_2) δ = 28−22 br. ^{13}C NMR (125 MHz, CD_2Cl_2) δ = 133.1 (s, C_6H_5), 130.7 (s, C_6H_5), 130.1 (s, C_6H_5), 128.5 (s, C_6H_5), 127.6 (s, C_6H_5), 126.7 (s, C_6H_5), 126.0 (s, C_6H_5), 26.6 (br, CH_2).

[X(CO)$_2$(dppe)WCC(Me)C(Me)CW(CO)$_2$(dppe)X] (5 (X = I), 6 (X = Cl)). Solid $[Me_3O]BF_4$ (7 mg, 0.046 mmol) was slowly added to the solution of **2** (40 mg, 0.023 mmol) and NBu_4I or

(59) *Stoe IPDS Software*, Version 2.87 5/1998 ed.; Stoe & Cie: Darmstadt, Germany, 1998.
(60) *CrysAlisPro*, Version 1.171.32.5 ed.; Oxford Diffraction Ltd.: Abingdon, Oxfordshire, England, 2007.
(61) Sheldrick, G. M. *Acta Crystallogr.* **2008**, *A64*, 112–122.
(62) Spek, A. L. *J. Appl. Crystallogr.* **2003**, *36*, 7–13.

NBu_4Cl (25 or 19 mg, 0.069 mmol) in glyme (2 mL) at −20 °C. Stirring of this mixture for 6 h led to the formation of a pale-orange precipitate (15 mg for I and 5 mg for Cl), which was filtered and dispersed in CH_2Cl_2 (8 mL). To this solution was added iodine (3 mg, 0.012 mmol) or $[FeCp_2]PF_6$ (2.6 mg, 0.008 mmol) in 2 mL of CH_2Cl_2. After stirring the reaction mixture for 1 h, the solvent was removed *in vacuo*, and the red-brown product obtained was crystallized from CH_2Cl_2/acetonitrile to give **5** and **6** as red crystals, respectively. Single crystals of **5** and **6** suitable for X-ray diffraction were grown by slow evaporation of CH_2Cl_2 from CH_2Cl_2/acetonitrile mixture. For **5**: Yield: 7 mg (0.0044 mmol, 20%). Anal. Calcd for $C_{62}H_{54}I_2O_4P_4W_2$: C, 46.30; H, 3.38. Found: C, 46.28; H, 3.60. IR (cm^{-1}): 1976 (CO), 1918 (CO). ^1H NMR (200 MHz, CD_2Cl_2) δ = 7.85−7.57 (m, 15H, C_6H_5), 7.44−7.34 (m, 25H, C_6H_5), 3.15 (m, 4H, CH_2), 2.75 (m, 4H, CH_2), 0.56 (s, 6H, CH_3). ^{31}P NMR (81 MHz, CD_2Cl_2) δ = 28.04. ^{13}C NMR (125 MHz, CD_2Cl_2) δ = 133.0 (s, C_6H_5), 132.3 (s, C_6H_5), 129.0 (m, C_6H_5), 128.5 (m, C_6H_5), 30.0 (m, CH_2), 10.7 (s, CH_3). For **6**: Yield: 1 mg (0.0007 mmol, 3%). Anal. Calcd for $C_{62}H_{54}Cl_2O_4P_4W_2$: C, 52.24; H, 3.82. Found: C, 52.47; H, 3.97. IR (cm^{-1}): 1983 (CO), 1921 (CO). ^1H NMR (200 MHz, CD_2Cl_2) δ = 7.82−7.57 (m, 15H, C_6H_5), 7.45−7.32 (m, 25H, C_6H_5), 2.97 (m, 4H, CH_2), 2.70 (m, 4H, CH_2), 0.53 (s, 6H, CH_3). ^{31}P NMR (81 MHz, CD_2Cl_2) δ = 38.19 (s, $^1J_{W-P}$ (d, satellite) = 230 Hz). ^{13}C NMR (125 MHz, CD_2Cl_2) δ = 132.7 (m, C_6H_5), 130.7 (s, C_6H_5), 130.0 (m, C_6H_5), 128.6 (m, C_6H_5), 26.3 (m, CH_2), 16.7 (s, CH_3).

[Cl(CO)$_2$(dppe)WC$_4$W(CO)$_2$(dppe)Cl] (7). Method 1: Chloroform (1 mL) was added to the solution of **2** (40 mg, 0.023 mmol) in diglyme (2 mL). The reaction mixture was kept at room temperature until a color change to dark violet was observed. After that the solvent was removed *in vacuo*. The reaction mixture was adsorbed onto silica gel and subjected to column chromatography using benzene as eluent to isolate a red band to give 6 mg (0.0034 mmol, 15%) of **7**. A pink powder was isolated after removal of the solvent and subsequent washing with acetonitrile and drying *in vacuo*. Method 2: A solution of C_2Cl_6 (12.15 mg, 0.053 mmol) in THF (1 mL) was added dropwise to a solution of **2** (40 mg, 0.023 mmol) in glyme (1 mL) at room temperature. After stirring the reaction mixture for 6 h, the solvent was removed *in vacuo*, and the red-brown product obtained was washed three times with 1 mL of acetonitrile and dried *in vacuo*. Single crystals suitable for X-ray diffraction were grown by layering a benzene solution with pentane. Yield: 17 mg (0.012 mmol, 51%). Anal. Calcd for $C_{60}H_{48}Cl_2O_4P_4W_2$: C, 51.64; H, 3.47. Found: C, 51.81; H, 3.71. IR (cm^{-1}): 1992 (CO), 1934 (CO). ^1H NMR (200 MHz, C_6D_6) δ = 7.75−7.54 (m, 15H, C_6H_5), 7.06−6.89 (m, 25H, C_6H_5), 2.55 (m, 4H, CH_2), 2.15 (m, 4H, CH_2); ^{31}P NMR (81 MHz, C_6D_6) δ = 37.46 (s, $^1J_{W-P}$ (d, satellite) = 226 Hz); ^{13}C NMR (125 MHz, C_6D_6) δ = 228.4 (s, C_α), 215.0 (dd, $^2J_{C-P(cis)}$ = 7.2 Hz, $^2J_{C-P(trans)}$ = 48.0 Hz, CO), 135.3−135.0 (d, $^1J_{C-P}$ = 42.5 Hz, *ipso*-C_6H_5), 133.5−133.2 (m, C_6H_5), 130.7−130.4 (d, $^3J_{C-P}$ = 40.4 Hz, *para*-C_6H_5), 128.7−128.6 (m, C_6H_5), 85.8 (s, C_β) 27.8 (dd, $^1J_{C-P}$ = 26 Hz, $^2J_{C-P}$ = 12.5 Hz, CH_2).

[(SCN)(CO)$_2$(dppe)WC$_4$W(CO)$_2$(dppe)(NCS)] (8). An excess of the AgSCN (50 mg, 0.16 mmol) was added to a THF solution (5 mL) of **3** (50 mg, 0.032 mmol). The reaction mixture was stirred for 18 h at 50 °C. The resulting brown suspension was filtered, and solvent was removed *in vacuo*. Complex **8** formed as violet needles after crystallization from CH_2Cl_2/pentane. Single crystals suitable for X-ray diffraction were grown by layering benzene solution with pentane. Yield: 24 mg (0.017 mmol, 52%). Anal. Calcd for $C_{62}H_{48}N_2O_4P_4S_2W_2$: C, 51.69; H, 3.36; N, 1.94. Found: C, 51.75; H, 3.46; N, 1.96. IR (cm^{-1}): 2034 (NCS), 1988 (CO), 1931 (CO). ^1H NMR (500 MHz, CD_2Cl_2) δ = 7.62−7.52 (m, 15H, C_6H_5), 7.49 (m, 10H, C_6H_5), 7.35−7.15 (m, 15H, C_6H_5), 2.88 (m, 4H, CH_2), 2.62 (m, 4H, CH_2). ^{31}P NMR (81 MHz, C_6D_5Cl) δ = 39.88 (s, $^1J_{W-P}$ = (d, satellite) 234 Hz). ^{13}C NMR (125 MHz, C_6D_5Cl)[63] δ = 232.1 (s, C_α), 210.8 (dd, $^2J_{C-P(cis)}$ = 7.1 Hz, $^2J_{C-P(trans)}$ = 50.0 Hz, CO), 143.8 (s, NCS), 134.0 (d, $^1J_{C-P}$ = 49.5 Hz, *ipso*-C_6H_5), 133.1 (d, $^NJ_{C-P}$ = 18.5 Hz, C_6H_5), 132.6 (d, $^NJ_{C-P}$ = 18.4 Hz, C_6H_5), 131.2 (s, C_6H_5), 130.9 (s, C_6H_5), 129.5 (d, $^NJ_{C-P}$ = 16.5 Hz, C_6H_5), 128.9 (d, $^NJ_{C-P}$ = 16.6 Hz, C_6H_5), 82.1 (s, C_β) 24.9 (dd, $^1J_{C-P}$ = 36 Hz, $^2J_{C-P}$ = 16.5 Hz, CH_2).

[(TfO)(CO)$_2$(dppe)WC$_4$W(CO)$_2$(dppe)(OTf)] (9). A solution of silver triflate (17 mg, 0.064 mmol) in THF (3 mL) was added dropwise to a solution of **3** (50 mg, 0.032 mmol) in THF (3 mL) at room temperature. After stirring the reaction mixture for 20 min, the solution was filtered and cooled to −30 °C to give **9** as pale-violet needles. Yield: 43 mg (0.026 mmol, 83%). Anal. Calcd for $C_{62}H_{48}F_6O_{10}P_4S_2W_2$: C, 45.89; H, 2.98; N. Found: C, 45.81; H, 3.07; IR (cm^{-1}): 2000 (CO), 1945 (CO). ^1H NMR (200 MHz, THF-d_8) δ = 7.68−7.59 (m, 15H, C_6H_5), 7.42−7.34 (m, 25H, C_6H_5), 2.96−2.85 (m, 8H, CH_2). ^{31}P NMR (81 MHz, THF-d_8) δ = 44.82 (s, $^1J_{W-P}$ = (d, satellite) 236 Hz). ^{19}F NMR (188 MHz, THF-d_8) δ = −79.31 (s, SO_3CF_3). ^{13}C NMR (125 MHz, CD_2Cl_2) 215.7 (dd, $^2J_{C-P(cis)}$ = 7 Hz, $^2J_{C-P(trans)}$ = 50.5 Hz, CO), 135.6 (d, $^1J_{C-P}$ = 45.6 Hz, *ipso*-C_6H_5), 133.8 (d, $^NJ_{C-P}$ = 11.7 Hz, C_6H_5), 133.4 (d, $^NJ_{C-P}$ = 11.5 Hz, C_6H_5), 131.6 (d, $^1J_{C-P}$ = 40.6 Hz, *ipso*-C_6H_5), 131.7 (s, C_6H_5), 129.9 (d, $^NJ_{C-P}$ = 10.2 Hz, C_6H_5), 129.6 (d, $^NJ_{C-P}$ = 10.5 Hz, C_6H_5), 82.1 (s, C_β) 28.2 (dd, $^1J_{C-P}$ = 29.0 Hz, $^2J_{C-P}$ = 11.2 Hz, CH_2).

[I(dppe)$_2$WC$_4$W(dppe)$_2$I] (10). **3** (300 mg, 0.192 mmol) and diphenylphosphinoethane (dppe) (450 mg, 1.13 mmol) in diglyme (21 mL) were placed into a Young−Schlenk tube. The mixture was heated at 140 °C for 7 days. The tube was evacuated three times during this time. Large dark-green crystals of **10** separated as the solution became more transparent. Single crystals suitable for X-ray diffraction were grown by layering a CH_2Cl_2 solution with pentane. Yield: 395 mg (0.174 mmol, 91%). Anal. Calcd for $C_{108}H_{96}I_2P_8W_2$: C, 57.32; H, 4.28. Found: C, 57.12; H, 4.14. IR (cm^{-1}): 1900 (C≡C). ^1H NMR (200 MHz, CD_2Cl_2): δ = 7.85 (br, 15H, C_6H_5), 7.26−6.76 (m, 65H, C_6H_5), 2.81 (m, 8H, CH_2), 1.82 (m, 8H, CH_2). ^{31}P NMR (81 MHz, C_6D_6): δ = 45 br. ^{13}C NMR (125 MHz, CD_2Cl_2) δ = 213.1 (m, C_α), 141.7 (br, *ipso*-C_6H_5), 139.9 (br, *ipso*-C_6H_5), 135.5 (s, C_6H_5), 134.0 (s, C_6H_5), 129.4 (s, C_6H_5), 126.8 (s, C_6H_5), 86.5 (s, C_β) 36.0 (m, CH_2).

[I(dppe)$_2$WC$_4$W(dppe)$_2$I][PF$_6$] (10[PF$_6$]). To a solution of **10** (40 mg, 0.0177 mmol) in 8 mL of dichloromethane was added dropwise a solution of $[FeCp_2][PF_6]$ (5.9 mg, 0.0177 mmol). The reaction mixture was stirred for 1 h, and the solvent was removed *in vacuo*. The resulting solid was washed with benzene to remove ferrocene and recrystallized by layering the CH_2Cl_2 solution with ether to give **10[PF$_6$]**. Yield: 25.5 mg (0.0106 mmol, 60%). Anal. Calcd for $C_{108}H_{96}I_2F_6P_9W_2$: C, 53.86; H, 4.02. Found: C, 53.97; H, 4.21. IR (cm^{-1}): 1891 (C≡C). ^1H NMR (200 MHz, CD_2Cl_2): δ = 8.54−7.03 (m, C_6H_5), 1.26 (br), 0.2 (br), −2.6 (br), −3.4 (br), −4.8 (br).

[I(dppe)$_2$WC$_4$W(dppe)$_2$I][PF$_6$]$_2$ (10[PF$_6$]$_2$). A solution of $[Ph_3C][PF_6]$ (14.3 mg, 0.0354 mmol) was added dropwise at −20 °C to a solution of **10** (40 mg, 0.0177 mmol) in 8 mL of dichloromethane. The reaction mixture was stirred for 10 min at room temperature, and the solvent was removed *in vacuo*. The resulting solid was washed with benzene and recrystallized by layering a CH_2Cl_2 solution with ether to give **10[PF$_6$]$_2$**. Yield: 24 mg (0.0094 mmol, 53%). Anal. Calcd for $C_{108}H_{96}I_2F_{12}P_{10}W_2$: C, 50.81; H, 3.79. Found: C, 50.69; H, 3.86. IR (cm^{-1}): 1892 (C≡C). ^1H NMR (200 MHz, CD_2Cl_2): δ = 9.12−7.2 (m, C_6H_5), 1.35 (br), −0.64 (br), −5.82 (br), −6.82 (br).

[I(dppe)$_2$WC$_4$W(dppe)(CO)$_2$I] (11). **3** (50 mg, 0.032 mmol) and diphenylphosphinoethane (dppe) (40 mg, 0.1 mmol) were placed into Young−Schlenk tube and dissolved in a mixture of 3 mL of THF with 0.3 mL of CH_3CN. This tube was irradiated by a 125 W

(63) The NMR ^{13}C signals of the phenyl groups of dppe were determined separately in CD_2Cl_2 solution. N = 2 for ortho carbons, 3 for meta carbons, 4 for para carbons. Unfortunately, reliable assignment is difficult in this case.

medium pressure UV lamp (six intervals, 10 min each). The reaction was monitored by ^{31}P NMR and stopped when the signal of **3** had disappeared. The reaction mixture was evaporated, washed with pentane, and subsequently subjected to flash chromatography (silica gel, benzene) to give 23 mg of **11**. It was recrystallized from benzene. Single crystals suitable for X-ray diffraction were grown by layering a benzene solution with pentane. Yield: 23 mg (0.012 mmol, 38%). Anal. Calcd for $C_{84}H_{72}I_2O_2P_6W_2$: C, 52.52; H, 3.78. Found: C, 52.37; H, 3.92. IR (cm^{-1}): 1987 (CO), 1922 (CO). ^{1}H NMR (200 MHz, C_6D_6): δ = 7.72−7.58 (m, 16H, C_6H_5), 7.27 (m, 8H, C_6H_5), 7.08 (m, 17H, C_6H_5), 6.95 (m, 15H, C_6H_5), 6.78 (m, 4H, C_6H_5), 2.91 (m, 6H, CH_2), 2.36 (m, 6H, CH_2). ^{31}P NMR (81 MHz, C_6D_6): δ = 31.74 (s, 2P, $^1J_{W-P}$ (d, satellite) = 230 Hz), 32.33 (s, 4P, $^1J_{W-P}$ = (d, satellite) 268 Hz). ^{13}C NMR (125 MHz, CD_2Cl_2) δ = 230.3 (s, C_α W(dppe)$(CO)_2$), 212.8 (dd, $^2J_{C-P(cis)}$ = 6.7 Hz, $^2J_{C-P(trans)}$ = 42.0 Hz, CO), 212.3 (s, C_α W$(dppe)_2$) 140.9−139.6 (m, *ipso*-C_6H_5), 136.1−134.9 (m, C_6H_5), 134.2 (s, C_6H_5), 133.8 (d, J_{C-P} = 12 Hz, C_6H_5), 132.7 (d, $^NJ_{C-P}$ = 10 Hz, C_6H_5), 130.1 (s, C_6H_5), 129.7 (s, C_6H_5), 128.9−128.7 (m, C_6H_5), 127.5 (s, C_6H_5), 93.9 (s, $C_{\beta1}$), 83.0 (s, $C_{\beta2}$), 36.0 (m, CH_2 W$(dppe)_2$), 28.6 (dd, $^1J_{C-P}$ = 27.7 Hz, $^2J_{C-P}$ = 11.9 Hz, CH_2 W(dppe)$(CO)_2$).

[I(dppe)$_2$WC$_4$W(dppe)(CO)$_2$I][PF$_6$] (11[PF$_6$]). A solution of $[FeCp_2][PF_6]$ (4.3 mg, 0.013 mmol) was added dropwise to a solution of **11** (25 mg, 0.013 mmol) in 5 mL of dichloromethane. The reaction mixture was stirred for 1 h, and the solvent was removed *in vacuo*. The resulting solid was washed with benzene to remove ferrocene and redissolved in 1 mL of THF. The solution was placed at −30 °C. Brown crystals of **11[PF$_6$]** appeared after one day. Yield: 20 mg (0.0097 mmol, 74%). Anal. Calcd for $C_{84}H_{72}I_2F_6O_2P_7W_2$: C, 48.84; H, 3.51. Found: C, 49.01; H, 3.65. IR (cm^{-1}): 2000 (CO), 1938 (CO). ^{1}H NMR (200 MHz, CD_2Cl_2): δ = 9.1−6.75 (br, C_6H_5), 2.81 (br, CH_2), 2.29 (br, CH_2).

Acknowledgment. We thank S. Weyeneth, F. Muranyi, and A. Tsirlin for help with the magnetic measurements. Funding from the Swiss National Science Foundation (SNSF) and from the University of Zürich are gratefully acknowledged.

Supporting Information Available: Details of X-ray experiments, crystallographic information files, ORTEP-like plots of **4**−**8**, **11[PF$_6$]**, CV of **10** in THF, temperature dependence of χ vs T for **10[PF$_6$]**, **11[PF$_6$]**, and **10[PF$_6$]$_2$**. This material is available free of charge via the Internet at http://pubs.acs.org.

JA909764X